Three-wave Lateral Shearing Interferometry With Partially Coherent Light

Victor Fors

Department of Electrical and Information Technology
Lund University

June 18, 2015

Preface

I was born in Luleå and am finishing my studies for a master's in Engineering physics at LTH in Lund. This is my master's thesis, which is the last step for getting my degree. For my thesis I returned to my hometown after finding an interesting sounding project at the Division of Fluid and Experimental Mechanics, at LTU in Luleå.

I want to thank my supervisor Mikael Sjödahl for the help with the thesis and giving me the opportunity to work with the subject matter. I want to thank my other supervisor Mats Gustafsson and my examiner Daniel Sjöberg, the last of whom got me interested in electromagnetic wave propagation through a course with that name. I want to thank my fellow master's thesis student Johan Öhman for bouncing ideas. Finally I want to thank Per Gren and Henrik Lycksam for helping me find my way in the lab.

Abstract

This thesis contains an examination of a method for quantitative phase imaging using lateral shearing interferometry. The focus is on how the degree of spatial coherence in the light source effect the image. The method is examined by first creating a simulation of the system, then looking at some analytical solutions for the interaction between some parameters, and finally conducting an experiment with a simplified implementation of the system.

One problem with classic holography is that it is very sensitive to vibrations, another is that you can get speckles due to using a temporally coherent light source. The method in this thesis uses lateral shearing, where the reference is not split ahead of the object. This has been shown to be more robust against vibrations.

The method works by translating part of a wavefront in a lateral direction, creating a kind of shear between original wavefront and the translated part. From the interference between the two the difference in phase can be extracted. The method used to extract the phase requires the wavefronts to be shifted in spatial frequency. It is shown that this allow one to perform the shear by defocusing after the frequency shift. This is indeed how the experimental setup demonstrated is implemented.

The simulation is built upon the theory of some simpler imaging theory and diffraction. Some significant time has been spent optimizing its implementation in Matlab. The simulation allows one to examine the statistical properties of the system with very little work.

The work method of creating a simulation and then solving analytically for some parameters complemented each other very well. When either does not agree with that of the other one immediately knows there is an error. The simulation also provides what parameters actually are important, so you do not have to do a lot of work that leads to boring conclusions.

Symbol and naming conventions

$\boldsymbol{r}$	Spatial vector
$\boldsymbol{\sigma}$	Spatial Frequency vector
$\boldsymbol{s}$	Normalized Spatial Frequency vector
u	Complex wave function (spatial domain)
U	Complex wave function (spatial frequency domain)
I	Intensity (spatial domain)
$\tilde{I}$	Intensity (spatial frequency domain)
J_{ij}	Mutual Intensity
μ_{ij}	Complex Coherence Factor
$\mathscr{G}$	Power Spectral Density
$\hat{\mathscr{G}}$	Normalized Power Spectral Density
$\mathscr{V}$	Visibility
NA	Numerical Aperture
λ	Wavelength of light
m	Magnification of the imaging system
z_1	Propagation distance, Object to Imaging system
z_2	Propagation distance, Imaging system to Detector
Δz_2	Defocus distance close to the image plane

Cartesian coordinate system is used $\{\hat{e}_x, \hat{e}_y, \hat{e}_z\}$ where $\hat{e}_z$ is the propagation direction along the length of the system. An arbitrary direction along the plane is referred to by non bold character without subscript, for example r. For circular symmetry the subscript $\perp$ is used as $\hat{e}_\perp = \sqrt{\hat{e}_x^2 + \hat{e}_y^2}$. The imaging system is split into three parts denoted object plane, aperture plane and image plane. The spatial bandwidth of the light is denoted by the superscript $\Delta\sigma^{BW}$ to keep it separated from a frequency shift $\Delta\sigma$. Functions can differ slightly in meaning depending on its inputs, for example the mutual intensity $J_{ij}(\boldsymbol{r})$ and the average mutual intensity $J_{ij} = \big\langle J_{ij}(\boldsymbol{r}) \big\rangle$.

Contents

CHAPTER 1

Introduction

Traditional *bright field microscopy* performs poorly when measuring transparent objects. *Phase-contrast microscopy* was invented in 1930s by Frits Zernike [1], for which he was awarded the Nobel prize. It allows the study of transparent objects by transforming changes in refractive index into amplitude changes in the image. The resulting images contain artifacts preventing them to be used quantitatively. In the 1950s, *differential interference contrast (DIC) microscopy* was invented by Georges Nomarski. It has been shown that this technique can give quantitative amplitude and phase measurement of the object [2]. One limitation of this technique is that it requires the use of polarized light, which makes it unsuitable for measuring objects that affect the polarization.

With the development of digital cameras and computational power, methods based on extracting information from interference patterns are possible. These work by using computational algorithms such as the fast Fourier transform (FFT) to acquire the amplitude and phase. For *digital holography*, one uses a reference-light that does not travel through the object you wish to measure [3]. In other words, you split the light up ahead of your object, and let one part pass through the object while the other goes around it. From the interference you can then extract the phase-shift caused by the object. An advantage of digital holography compared to many other methods is that you acquire the complex wave function. This allows you to refocus on different depths in the object by propagating the wave numerically [4]. One problem with this method is that it is sensitive to vibrations. In this thesis, a method that should be more robust and less sensitive is examined.

The type of system to be examined in this thesis is referred to as a *lateral shearing interferometer*. In these you split the light and translate the parts laterally away from each other, creating what is referred to as a *lateral shear* between the parts. Unlike classic digital holography the light can be split after it has passed the sample. This has been shown to be more robust and make the system less sensitive than the setup used for digital holography. As a consequence of not having the reference go around the object, the phase gradient is measured rather than the absolute phase. An advantage

of measuring the gradient is that it is easier to see fast changes in refractive index. One disadvantage is that you need to split the light more than once to get the gradient in more than one direction. Another disadvantage is that additional work is required to refocus numerically like in digital holography, as you do not directly acquire the complex wave function. There are a lot of different implementations of these systems, one example can be found in reference [5].

The work of this thesis was done at LTU (*Luleå university of technology*). A student project at LTU has earlier examined a similar system to the one examined in this thesis [6]. The problem that occurred was that the light was either not coherent enough for interference to occur, or it was too coherent such that speckles dominated the image. A point of focus is therefore to determine the effect the lights coherence has on the system. In a wider sense, the aim of the thesis is to in a quantitative way evaluate the qualities of the system. The work done for the thesis also provides simulation tools for further studies of similar systems.

The thesis uses three ways to examine the system. First, a simulation is created, then, parameters that affect the image are found and evaluated, finally, an experiment is conducted to validate the findings.

1.1 System Description

The lateral shearing interferometer examined in this thesis can be split up into three parts of interest. The *object plane*, the *aperture plane*, and the *image plane*. In the object plane, the source light gains a deterministic phase shift. The aperture plane consists of an imaging system to focus the light and optical components to split and shift the wave laterally in spatial frequency and space. The image plane is located close to the focus of the imaging system. The planes are illustrated in figure 1.1.

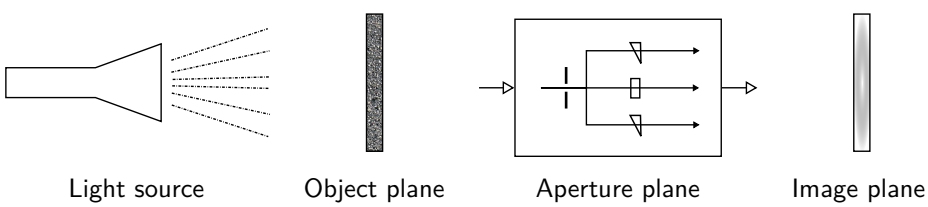

Figure 1.1: *Illustration of the system.*

The objective of the system is to measure the optical path difference of an object. This is achieved by splitting the wavefront into three identical wavefronts. One is used as *reference*, the other two act as *referents* and are sheared in the plane. The interference between the reference and a referent contains information about the phase difference in the direction of the shear. With the referents sheared in orthogonal directions information about the total phase gradient in the plane is available. To separate the interference terms the reference and referents are limited by an aperture and shifted in spatial frequency.

The step-by-step effect the system has on a wave front is illustrated in figure 1.2. In the first row of images, the wavefront coming from the object has been limited in spatial frequency by an aperture. The second row shows the wavefront being split

into the reference and two referents, with the referents shifted in spatial frequency. The third row introduces a lateral shear, where the referents are moved in the spatial domain. The fourth row shows the resulting intensity. See the theory presented in chapter 2 for a more in-depth description of these operations.

In short, the first two steps in figure 1.2, that limit and shift spatial frequency, are necessary in order to separate the lobes in the intensity. Because the intensity correspond to a convolution in the spatial frequency domain, the interference between the three wavefronts are separated into three pairs of lobes. A pair of interference lobes will be placed at the same distance from the center lobe, as the two wavefronts that make them up are separated in spatial frequency, see section 2.2. As an interference lobe contains information about the phase difference between the two wavefronts that make it up, the third step, the shear, make it contain information about a phase gradient.

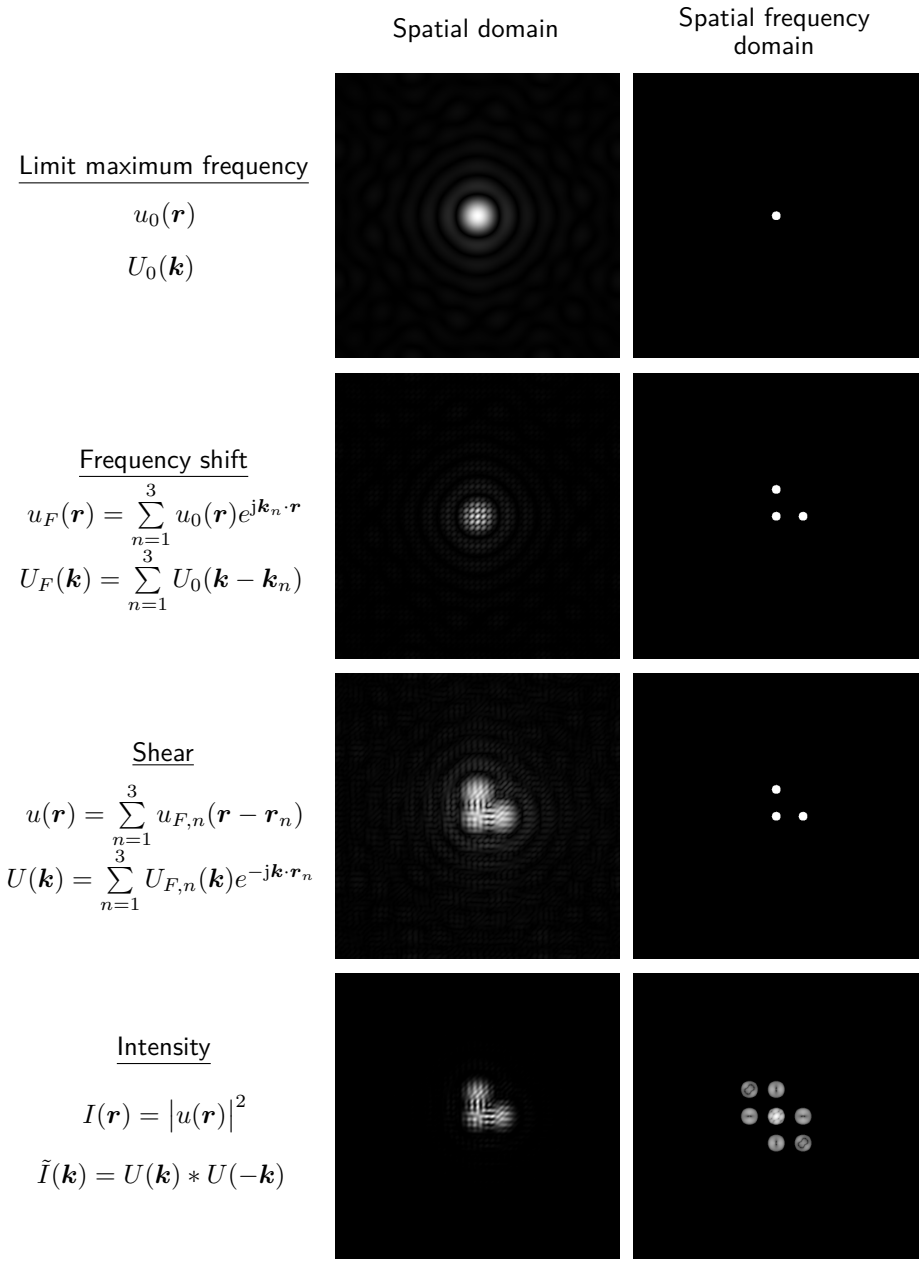

Figure 1.2: *Illustration of the effect of the system in the two domains. The top six images show the absolute value of the complex wave function for each step of the process in the aperture plane. The bottom two images show the final intensity. Corresponding mathematical expressions in both domains are written to the left of the images, starting from a wavefront limited in spatial frequency.*

CHAPTER 2

Theory

In this chapter the theory for understanding the concept of the imaging system is described. In order to determine how the resulting image quality depends on a set of parameters, there is a more in-depth look at some parts of the analytical model describing the system in chapter 4.

2.1 Interference

This section describes how information of the phase gradient is included in the interference between the reference and referents. The light is assumed to be monochromatic or quasi-monochromatic [7, p. 200]. This makes it possible to describe the light as a *wavefront*, where the temporal part of the wave is ignored. We also limit ourselves to a plane $\boldsymbol{r} = (r_x, r_y)$ with its normal in the direction of propagation $\hat{e}_z$. The complex wave function can then be described by its amplitude $A(\boldsymbol{r})$ and phase $\phi(\boldsymbol{r})$

$$u(\boldsymbol{r}) = A(\boldsymbol{r})e^{\mathrm{j}\phi(\boldsymbol{r})}, \tag{2.1-1}$$

where $A(\boldsymbol{r}) = \left|u(\boldsymbol{r})\right|$, and $\phi(\boldsymbol{r}) = \arg u(\boldsymbol{r})$. We define the *intensity* of a wavefront

$$I(\boldsymbol{r}) \equiv u(\boldsymbol{r})u^*(\boldsymbol{r}) = \left|A(\boldsymbol{r})\right|^2, \tag{2.1-2}$$

and the *mutual intensity* between two wavefronts

$$\begin{aligned} J_{ij}(\boldsymbol{r}) &\equiv u_i(\boldsymbol{r})u_j^*(\boldsymbol{r}) \\ &= A_i(\boldsymbol{r})A_j(\boldsymbol{r})e^{\mathrm{j}\left(\phi_i(\boldsymbol{r})-\phi_j(\boldsymbol{r})\right)} \\ &= \sqrt{I_i(\boldsymbol{r})I_j(\boldsymbol{r})}e^{\mathrm{j}\left(\phi_i(\boldsymbol{r})-\phi_j(\boldsymbol{r})\right)}. \end{aligned} \tag{2.1-3}$$

If $i = j$ we get $I_i(\boldsymbol{r}) = J_{ii}(\boldsymbol{r})$. It's also easily seen that $J_{ij}(\boldsymbol{r}) = J_{ji}^*(\boldsymbol{r})$. For three interfering wavefronts u_1, u_2 and u_3 the *total intensity* is

$$\begin{aligned} I(\boldsymbol{r}) &= u(\boldsymbol{r})u^*(\boldsymbol{r}) \\ &= (u_1(\boldsymbol{r}) + u_2(\boldsymbol{r}) + u_3(\boldsymbol{r}))(u_1(\boldsymbol{r}) + u_2(\boldsymbol{r}) + u_3(\boldsymbol{r}))^* \\ &= I_1(\boldsymbol{r}) + I_2(\boldsymbol{r}) + I_3(\boldsymbol{r}) \\ &+ J_{12}(\boldsymbol{r}) + J_{13}(\boldsymbol{r}) + J_{23}(\boldsymbol{r}) \\ &+ J_{12}^*(\boldsymbol{r}) + J_{13}^*(\boldsymbol{r}) + J_{23}^*(\boldsymbol{r}). \end{aligned} \tag{2.1-4}$$

In words, the total intensity can be described as the sum of individual intensities I_i and mutual intensities J_{ij} for all combination i and j. Each individual mutual intensity terms is complex, but due to the conjugate terms being present the total intensity is real. It is the individual mutual intensity terms that are able to hold information about the phase. If $u_1 = u_0(r_x, r_y)$ is the reference, $u_2 = u_0(r_x + \Delta r_x, r_y)$ the referent sheared in e_x, and $u_3 = u_0(r_x, r_y + \Delta r_y)$ the referent sheared in e_y, $J_{12}(\boldsymbol{r})$ and $J_{13}(\boldsymbol{r}, t)$ contain two orthogonal phase gradients

$$\arg J_{12}(\boldsymbol{r}) = \phi_1 - \phi_2 = \phi_0(r_x, r_y) - \phi_0(r_x + \Delta r_x, r_y), \tag{2.1-5}$$

$$\arg J_{13}(\boldsymbol{r}) = \phi_1 - \phi_3 = \phi_0(r_x, r_y) - \phi_0(r_x, r_y + \Delta r_y). \tag{2.1-6}$$

2.2 Extraction of Mutual Intensity

As it is only possible to measure the intensity you need to use some way to separate the mutual intensity terms of interest. There are multiple methods of doing so [8]. In this system, we separate the three wavefronts in spatial frequency, which we will see makes it possible to separate the mutual intensity terms. The *power spectral density* is defined as the two-dimensional Fourier transform of the mutual intensity

$$\begin{aligned} \mathscr{G}_{ij}(\boldsymbol{\sigma}) &= \mathscr{F}[J_{ij}(\boldsymbol{r})] \\ &= \mathscr{F}[u_i(\boldsymbol{r})u_j^*(\boldsymbol{r})] \\ &= \mathscr{F}[u_i(\boldsymbol{r})] * \mathscr{F}[u_j^*(\boldsymbol{r})] \\ &= U_i(\boldsymbol{\sigma}) * U_j^*(-\boldsymbol{\sigma}) \\ &= \iint_{-\infty}^{\infty} U_i(\tau_x, \tau_y) U_j^*(-\sigma_x - \tau_x, -\sigma_y - \tau_y)\,\mathrm{d}\tau_x\,\mathrm{d}\tau_y. \end{aligned} \tag{2.2-1}$$

where $\boldsymbol{\sigma}$ is a spatial frequency vector in the plane. For $i = j$ we get the intensity in the spatial frequency domain $\tilde{I}_i = \mathscr{G}_{ii}$. From $J_{ij}(\boldsymbol{r}) = J_{ji}^*(\boldsymbol{r})$ we get $\mathscr{G}_{ij}(\boldsymbol{\sigma}) = \mathscr{G}_{ji}^*(-\boldsymbol{\sigma})$. For three interfering wavefronts $U_1(\boldsymbol{\sigma})$, $U_2(\boldsymbol{\sigma})$ and $U_3(\boldsymbol{\sigma})$, we get the total intensity

$$\begin{aligned} \tilde{I}(\boldsymbol{\sigma}) &= U(\boldsymbol{\sigma}) * U^*(-\boldsymbol{\sigma}) \\ &= (U_1(\boldsymbol{\sigma}) + U_2(\boldsymbol{\sigma}) + U_3(\boldsymbol{\sigma})) * (U_1(-\boldsymbol{\sigma}) + U_2(-\boldsymbol{\sigma}) + U_3(-\boldsymbol{\sigma}))^* \\ &= \tilde{I}_1(\boldsymbol{\sigma}) + \tilde{I}_2(\boldsymbol{\sigma}) + \tilde{I}_3(\boldsymbol{\sigma}) \\ &+ \mathscr{G}_{12}(\boldsymbol{\sigma}) + \mathscr{G}_{13}(\boldsymbol{\sigma}) + \mathscr{G}_{23}(\boldsymbol{\sigma}) \\ &+ \mathscr{G}_{12}^*(-\boldsymbol{\sigma}) + \mathscr{G}_{13}^*(-\boldsymbol{\sigma}) + \mathscr{G}_{23}^*(-\boldsymbol{\sigma}). \end{aligned} \tag{2.2-2}$$

In order to separate the power spectral densities in the spatial frequency domain they must be limited in spatial frequency. We achieve this by limiting the wavefronts to a maximum frequency σ_{max} (see section 2.4) and then shifting them in spatial frequency. To see what effect this has on the power spectral density, we for simplicity first consider the one dimensional integral

$$\begin{aligned}
&\int_{-\infty}^{\infty} f(\tau,\sigma)\,\mathrm{rect}\left(\frac{\tau-\Delta\sigma_i}{2\sigma_{max}}\right)\mathrm{rect}\left(\frac{-\sigma-\tau+\Delta\sigma_j}{2\sigma_{max}}\right)\mathrm{d}\tau \\
&= \begin{cases}
\int_{\Delta\sigma_i-\sigma_{max}}^{\Delta\sigma_j+\sigma_{max}} f(\tau,\sigma)\,\mathrm{d}\tau, & -\Delta\sigma_i+\Delta\sigma_j-2\sigma_{max}<\sigma<-\Delta\sigma_i+\Delta\sigma_j \\
\int_{\Delta\sigma_j-\sigma-\sigma_{max}}^{\Delta\sigma_i+\sigma_{max}} f(\tau,\sigma)\,\mathrm{d}\tau, & -\Delta\sigma_i+\Delta\sigma_j<\sigma<-\Delta\sigma_i+\Delta\sigma_j+2\sigma_{max} \\
0, & \left|\sigma+\Delta\sigma_i-\Delta\sigma_j\right|>2\sigma_{max}
\end{cases},
\end{aligned} \tag{2.2-3}$$

where $\Delta\sigma_i$ and $\Delta\sigma_j$ are frequency shifts and rect is the rectangle function

$$\mathrm{rect}(x)=\begin{cases}0, & |x|>1/2\\ 1, & |x|<1/2\end{cases}. \tag{2.2-4}$$

With the help of equation (2.2-3) and equation (2.2-1), one can see that the power spectral density between two wavefronts limited and then shifted in frequency can be written

$$\mathscr{G}_{ij}(\boldsymbol{\sigma})=\begin{cases}U_i(\boldsymbol{\sigma}-\Delta\boldsymbol{\sigma}_i)*U_j^*(-\boldsymbol{\sigma}+\Delta\boldsymbol{\sigma}_j), & \left|\boldsymbol{\sigma}+\Delta\boldsymbol{\sigma}_i-\Delta\boldsymbol{\sigma}_j\right|<2\sigma_{max}\\ 0, & \left|\boldsymbol{\sigma}+\Delta\boldsymbol{\sigma}_i-\Delta\boldsymbol{\sigma}_j\right|>2\sigma_{max}\end{cases}, \tag{2.2-5}$$

where $\Delta\boldsymbol{\sigma}_i$ and $\Delta\boldsymbol{\sigma}_j$ are the lateral frequency shifts of the wavefronts after the frequencies above σ_{max} have been removed. We can see that for $i=j$, the power spectral density has its center at the zero frequency with a radius of $2\sigma_{max}$. For $i\neq j$, it is only the relative difference in spatial frequency between the two wavefronts that matter for where in the spectra the power spectral densities is placed. The wavefronts in equation (2.2-2) thus need to be separated by at least $4\sigma_{max}$ in order for the mutual intensities to not overlap. See figure 2.1 and 1.2.

2.3 Coherence

One usually splits up coherence into spatial coherence and temporal coherence. In this system we mainly concern ourselves with spatial coherence and assume the light to be quasi-monochromatic. If a wavefront is spatially coherent its phase is the same in the whole plane (planewave). The object will of course add phase shifts to the light, these phase shifts being what we want to image. We introduce the *phase error* ϕ_e, which is the random phase distribution due to partial incoherence in the light. First we look were it fits in the mutual intensity from equation 2.1-3

$$\begin{aligned}
J_{ij}(\boldsymbol{r}) &= \sqrt{I_i(\boldsymbol{r})I_j(\boldsymbol{r})}e^{\mathrm{j}\left(\phi_i(\boldsymbol{r})-\phi_j(\boldsymbol{r})\right)} \\
&= \sqrt{I_i(\boldsymbol{r})I_j(\boldsymbol{r})}e^{\mathrm{j}\left(\phi(\boldsymbol{r})+\phi_e(\boldsymbol{r})\right)},
\end{aligned} \tag{2.3-1}$$

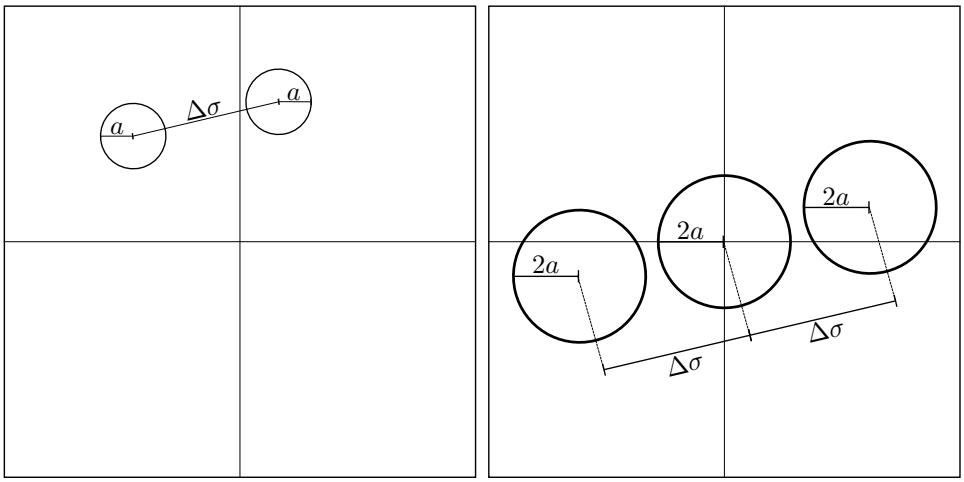

Figure 2.1: *Illustration of the spatial frequency domain for the interference between two wavefronts. The left box shows the complex wave functions and the right box shows the total intensity. The grids mark the origin. In this figure,* $a = \sigma_{max}$.

where ϕ is the deterministic contribution to the phase difference. When we have spatially coherent light the phase error $\phi_e(\boldsymbol{r}) = 0$. For incoherent light the phase error is uniformly random between $-\pi$ and π. For partially coherent light the phase error has a non uniform distribution. An example of how the phase error distribution for partially coherent light might look can be seen in figure 2.2.

The amplitude of the partially coherent light will also have a random distribution. This will create speckles in the intensity, which is commonly referred to as a *speckle pattern* and is the term we will use for one random distribution of the phase and amplitude. To get rid of the phase error we introduce a bit of temporal incoherence. By integrating over some time we will effectively sum multiple uncorrelated speckle patterns, where the number of uncorrelated speckle patterns depend on the temporal coherence and the integration time. We are interested of the sum of mutual intensities, which we write as the phasor sum

$$\alpha e^{\mathrm{j}\theta_e} e^{\mathrm{j}\phi} = \sum_{k=1}^{N} \alpha_k e^{\mathrm{j}\phi_e^k} e^{\mathrm{j}\phi} \tag{2.3-2}$$

where $\alpha_k = \sqrt{I_i^k(\boldsymbol{r}) I_j^k(\boldsymbol{r})}$, α is a real number, ϕ_e^k is the phase error of a single uncorrelated speckle pattern and θ_e is the new phase error after the summation of phasors. If the distribution of phases is around zero, the sum of random phasors will go towards a real positive number, and furthermore, it will go towards a normal distribution [9].

The degree of coherence can be measured using the *complex coherence factor* defined in [9, p.181]

$$\mu_{ij} \equiv \frac{\langle J_{ij}(\boldsymbol{r}) \rangle}{\sqrt{I_i I_j}}. \tag{2.3-3}$$

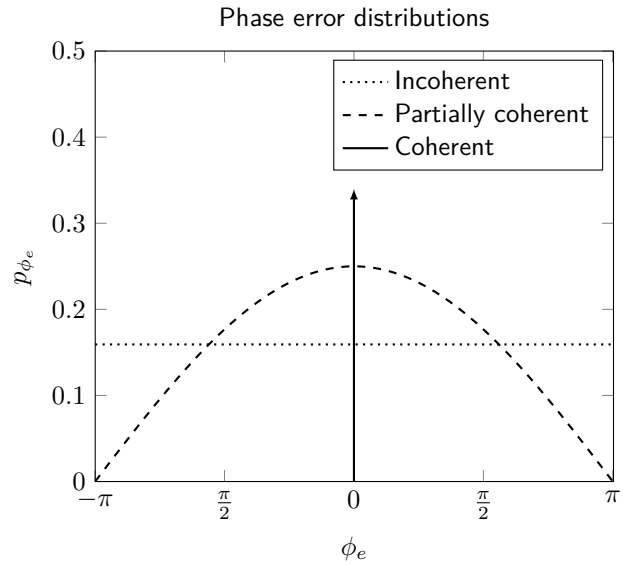

Figure 2.2: *Phase error distribution functions. The arrow represents the Dirac delta distribution function for coherent light.*

where we consider the *average mutual intensity* at all points in the plane, and where the intensities I_i and I_j are the average intensities over the whole plane. The absolute value of the complex coherence factor is clearly a number between zero and one. If we have spatially coherent light such that all points in the plane have the same phase, the absolute value of the complex coherence factor will equal one. And if we have incoherent light such that all points in the plane have a completely uncorrelated phase, the absolute value of the complex coherence factor will equal zero.

2.4 Imaging

To tie the operations in figure 1.2 to a physical system we will consider a 4-f telecentric imaging system [10]. Such a system recreates the object plane in the image plane without any optical aberrations (distortions), and can thus be described by its magnification and accepted frequencies. The *magnification* of this system is

$$m = -\frac{f_2}{f_1}, \tag{2.4-1}$$

where f_1 is the focal length of the entrance pupil, f_2 is the focal length of the exit pupil, and the minus sign is equivalent to a rotation of the image around $\hat{e}_z$ by 180 degrees. The spatial frequencies accepted by the system is described by the *numerical aperture* in object space

$$NA_0 \equiv \max s_\perp, \tag{2.4-2}$$

where $s_\perp = \lambda\sigma_\perp$ and $\lambda \max s_\perp = \sigma_{max}$ from section 2.2. The maximum directional cosines available to build up the image is then similarly described by the *numerical aperture* in image space

$$NA_1 \equiv -\frac{NA_0}{m}. \tag{2.4-3}$$

Because of the frequency shifts between the lenses there will however be larger frequencies present in the image plane (see section 2.2). Figure 2.3 shows an illustration that describes relevant parameters for the imaging. Because the wavefront will be

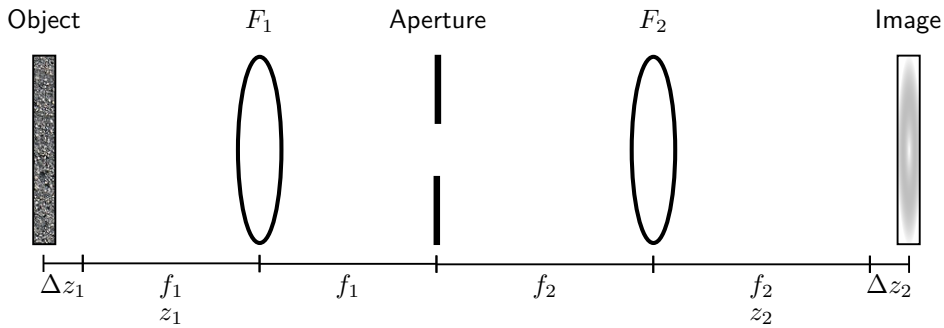

Figure 2.3: *Illustration of the 4-f telecentric imaging system. Components for lateral shear and frequency shift are not included in this illustration.*

further manipulated in between the lenses we have to differ between defocus in the object plane and the image plane. The distance between the object plane and the *entrance pupil* F_1 is therefore defined as $z_1 = f_1$, where f_1 is the focal length of F_1. Similarly the distance between the *exit pupil* F_2 and the image plane is defined as $z_2 = f_2$, where f_2 is the focal length of F_2. Defocus distances Δz_1 and Δz_2 are then used to account for offsets from these focus points. Generally, Δz_1 is assumed to be zero. A simple implementation of a system like this can be found in section 5.1.

CHAPTER 3

Simulation

The simulation provides a numerical solution to the system. It can be used to examine an experimental setup before building it, or for investigative work on how the system reacts to different changes in parameters. The full code for the Matlab implementations mentioned can be found in appendix A.

3.1 Numerical calculation of mutual coherence factor

Apart from simulating the full system it is expected to be of interest for how the mutual coherence function is affected by lateral shear. When the source light hits the object it is important that two points a set shearing distance apart is correlated enough for information about the phase gradient between these points be taken up by the wavefront. The goal is to implement equation (2.3-3) as a numerical function for all shears Δr_x and Δr_y. This corresponds to calculating and normalizing the autocorrelation of the wavefront.

In short, the implementation works by expanding the built-in two-dimensional cross-correlation function in Matlab *xcorr2.m*, to normalize with the intensities according to equation (2.3-3). Thankfully it is possible to optimize the calculations of the intensities so that they are significantly faster than the calculation of the correlations. As an optimization the maximum lag (shear) to be calculated has also been included as an input.

The speckle pattern is generated by randomizing spatial frequencies and performing a Fourier transform. One such speckle pattern has random spatial frequencies within the square area spanned by $\Delta\sigma_x^{BW}$ and $\Delta\sigma_y^{BW}$ (*Bandwidth* BW). The result of the normalized autocorrelation for such a matrix can be seen in figure 3.1. The analytical solutions for these specific speckle patterns are solved in section 4.1. Another intresting speckle pattern has random spatial frequencies within the area spanned by the circle with diameter $\Delta\sigma_\perp^{BW}$. The result of the normalized autocorrelation for such a matrix can be seen in figure 3.2.

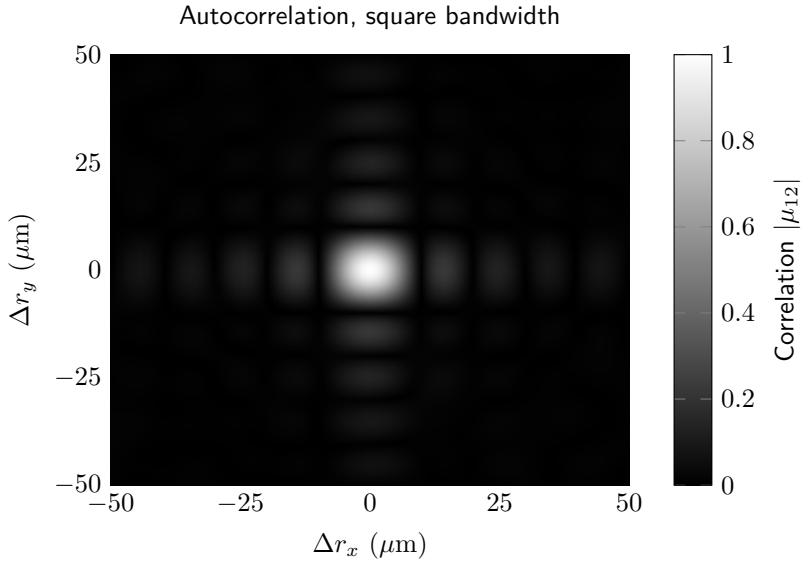

Figure 3.1: *The autocorrelation of square bandwidth in two dimensions. The maximum spatial frequency of the speckle pattern is* $\Delta\sigma_x^{BW} = \Delta\sigma_y^{BW} = 1/(10\mu m)$.

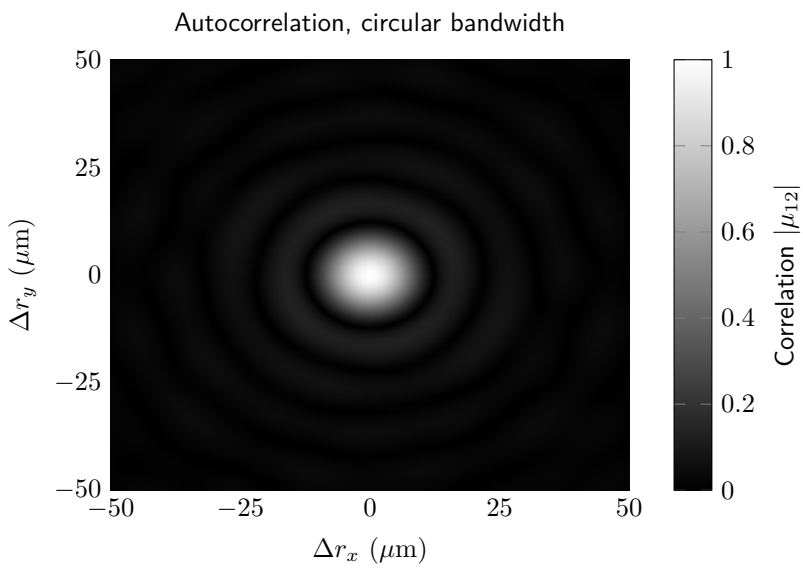

Figure 3.2: *The autocorrelation of circular bandwidth in two dimensions. The maximum spatial frequency of the speckle pattern is* $\Delta\sigma_\perp^{BW} = 1/(10\mu m)$.

3.2 Simulation of three-wave lateral shearing

The main work of this thesis was creating this simulation. The simulation is used to cross-check the validity of itself and some analytical models in chapter 4.

The simulation rests on very simple theory. It uses the imaging theory described in section 2.4, and it uses the *shift theorem* for diffraction and lateral shear.

The shift theorem in two dimensions can be written [11, p.244]

$$\mathscr{F}\left[u(\boldsymbol{r}+\Delta\boldsymbol{r})\right](\boldsymbol{\sigma}) = e^{\mathrm{j}2\pi\boldsymbol{\sigma}\,\Delta\boldsymbol{r}}\mathscr{F}\left[u(\boldsymbol{r})\right](\boldsymbol{\sigma}). \tag{3.2-1}$$

To diffract we translate in the direction of the normal to the plane. We can translate the spatial frequencies of the light in the plane $\{e_x, e_y\}$ to $\{e_z\}$ with

$$s_z = \sqrt{1 - s_x^2 - s_y^2} \tag{3.2-2}$$

where $\boldsymbol{s} = \lambda\boldsymbol{\sigma}$. Which concludes the theory needed for the simulation.

3.2.1 Implementation

The simulation can be described by the following steps:

1. Perform Fourier transform.
2. Remove frequencies filtered by the aperture.
3. Clone the wavefront.
4. Multiply each new wavefront with their relative part of the amplitude.
5. Shear each new wavefront using the shift theorem.
6. Shift each new wavefront in frequency by padding and shifting their matrices.
7. Sum all new wavefronts together.
8. Diffract according to defocus in image plane.
9. Flip sign of $\boldsymbol{\sigma}$.
10. Perform inverse Fourier transform.
11. Divide by the magnification and multiply by the phase factor matching the distance traveled by the wavefront.

One can note that the simulation in its current implementation does not perform any defocus close to the object. This is easily implemented but left out to simplify input. Currently all defocus is assumed to be close to the image plane. Note that because of the manipulation of the spatial frequencies of the split wavefronts, a defocus in the object plane can not be simulated through a defocus in the image plane. The reason that the frequency is not shifted using the shift theorem is that it would come with a very heavy performance cost.

Some amount of work was put into optimization. The three most important optimizations used are:

1. Minimized calculation grids. Filtering out higher frequencies is an apt opportunity to also decrease the size of the calculation grid without loss in precision.

2. Using Matlab native frequency mapping for Fourier transform. By default the built-in FFT-function i Matlab gives a vector containing the positive frequencies followed by the negative frequencies. It is common to use the Matlab function *fftshift.m* to shift the frequencies into a more natural order with the negative frequencies followed by the positive, making the center frequency the zero-frequency. *fftshift.m* is however very slow for complex matrices and performing index mapping in Matlab is well supported making *fftshift.m* redundant unless you mean to plot the frequencies.

3. The Matlab built-in *bsxfun.m* is used a lot and is a function for performing element-wise operations between different sized matrices. It makes vectorization easy while allowing you to keep the operators small.

3.2.2 Simulation example

The simulation was run with a wide variation of settings, trying to find qualitative relations between different parameters and image quality. Chapter 4 contains a quantitative study of the conclusions drawn from the simulation. To show the qualitative aspects of the simulation, figure 3.3 to figure 3.10 shows an example of a simulation run. As input, random speckle patterns with circular bandwidth such as in section 3.1 are given a deterministic phase shift consisting of some spherical objects. A new uncorrelated speckle pattern is generated for each iteration. The image is sheared by 1 mm defocus rather than direct shear (see section 4.5). Spatial frequencies are shifted such that the mutual intensity lobes doesn't overlap and in orthogonal directions in the way described by equation (4.5-12). A number of the settings used are listed in table 3.1.

Parameters	
Wavelength λ	633 nm
Focal length f	81 mm
Defocus Δz	1 mm
Shear Δr	0 mm
Numerical Aperture NA	0.0115
Frequency shift Δs	$4NA$
Speckle Bandwidth $\Delta\sigma^{bw}$	0.0096
Source resolution	1.66x1.66 µm
Iterations N	100

Table 3.1: *Some parameters used for the simulation example.*

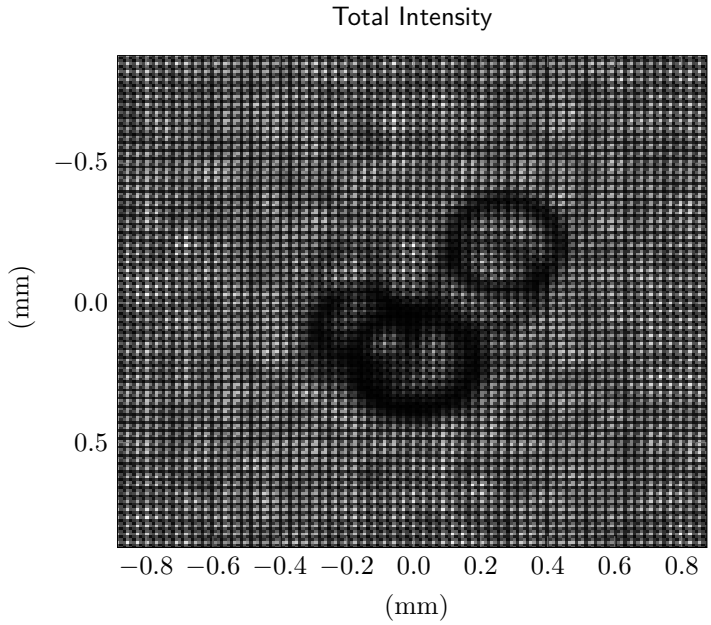

Figure 3.3: *Total Intensity from summation of 100 iterations.*

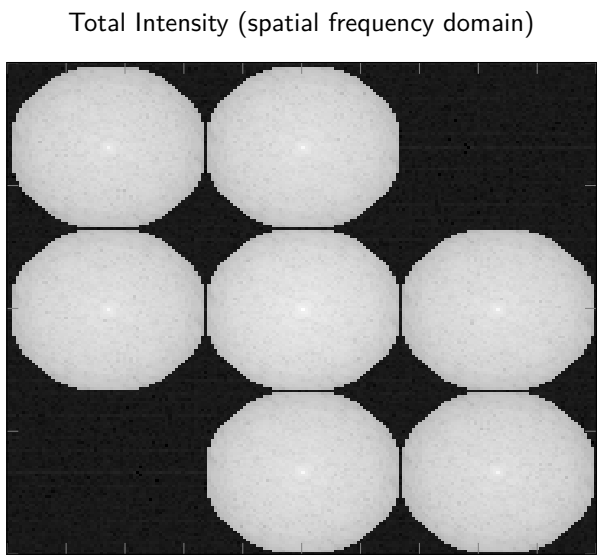

Figure 3.4: *Fourier transform of figure 3.3. The image shows the logarithmic absolute values. Compare to figure 1.2.*

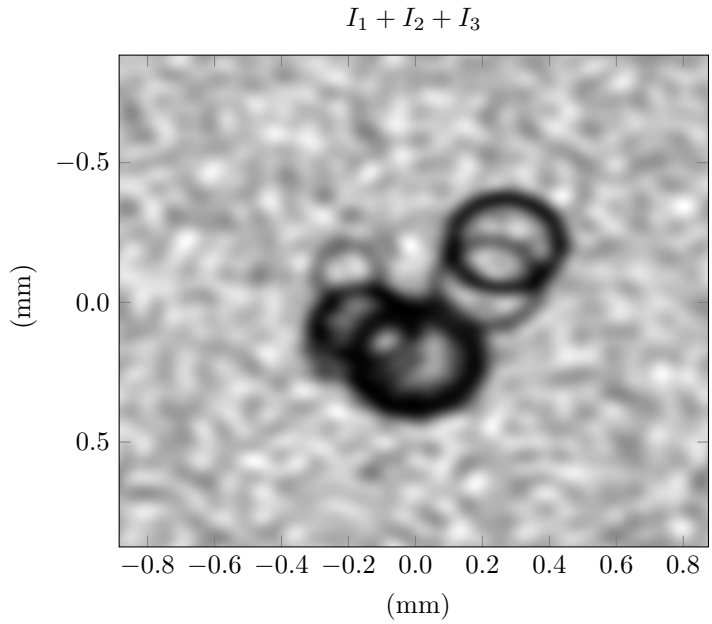

Figure 3.5: *Sum of the intensities. Extracted by filtering out all but the center lobe in figure 3.4.*

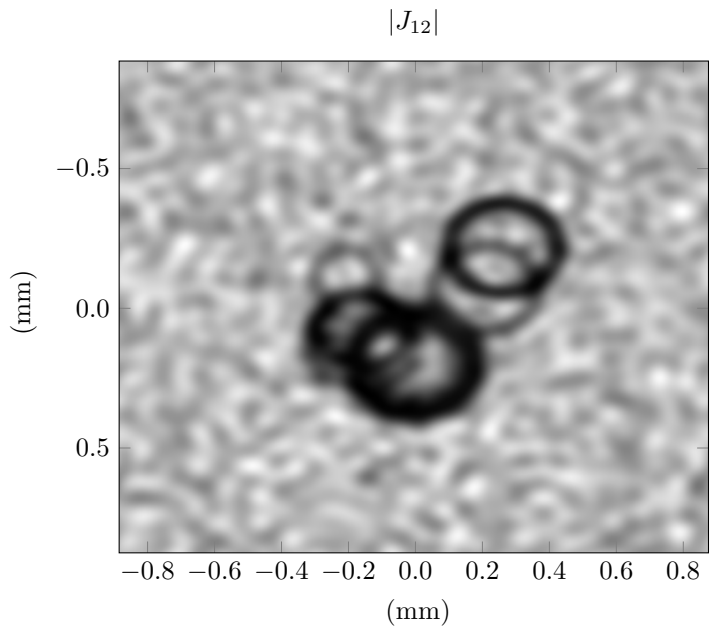

Figure 3.6: *Absolute value of Mutual intensity. Extracted by filtering out all but the center-right lobe in figure 5.6 and taking the absolute value.*

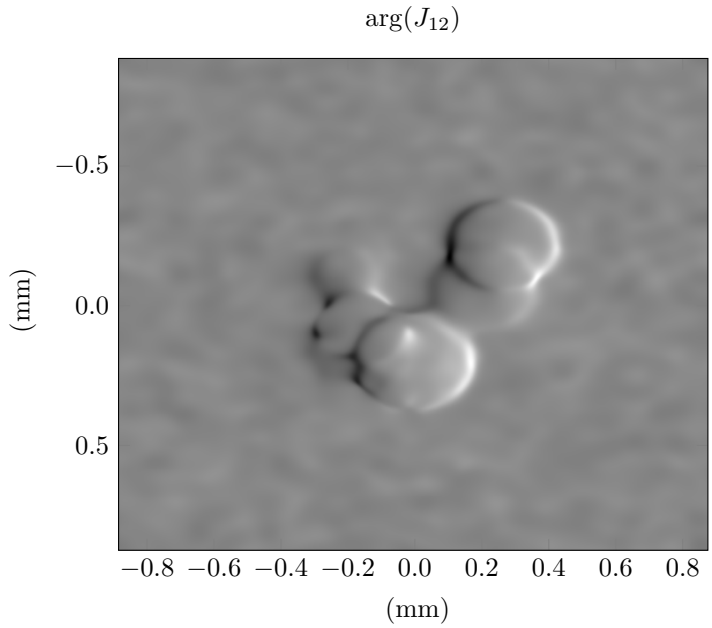

Figure 3.7: *Phase gradient in e_x. Extracted by filtering out all but the center-right lobe in figure 3.4 and taking the argument.*

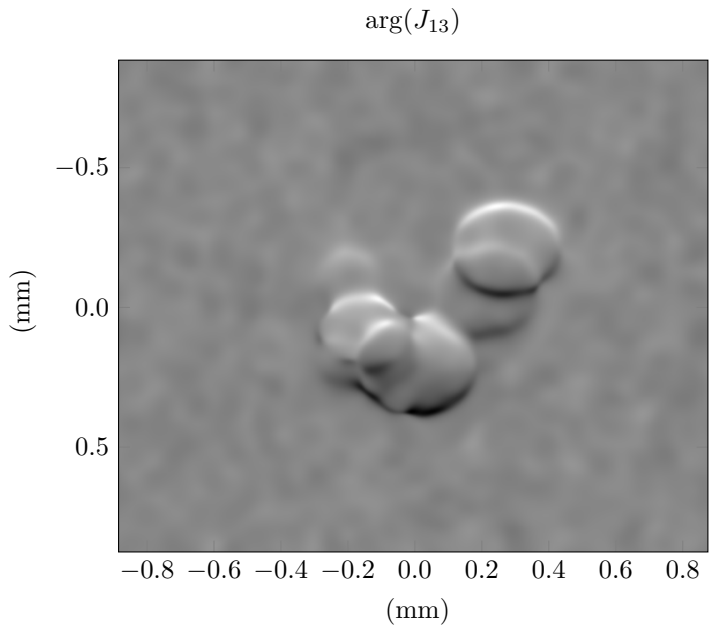

Figure 3.8: *Phase gradient in e_y. Extracted by filtering out all but the center-top lobe in figure 3.4 and taking the argument.*

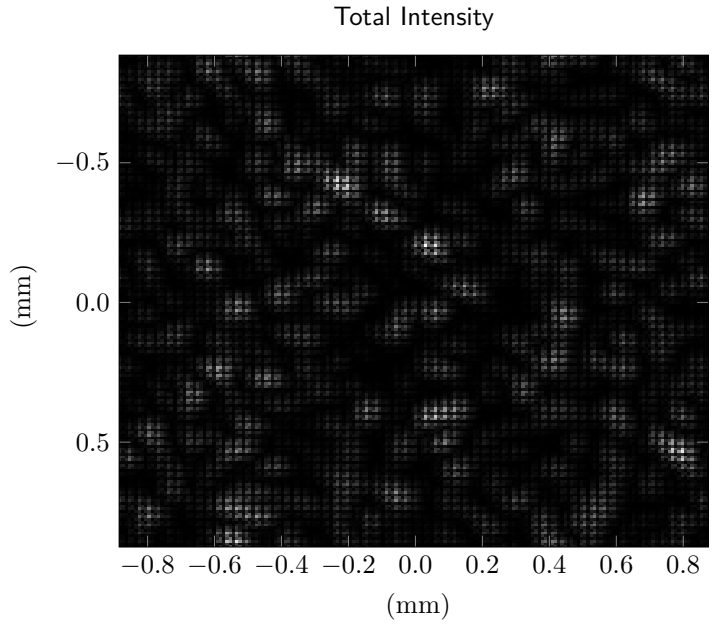

Figure 3.9: *Total Intensity from one iteration.*

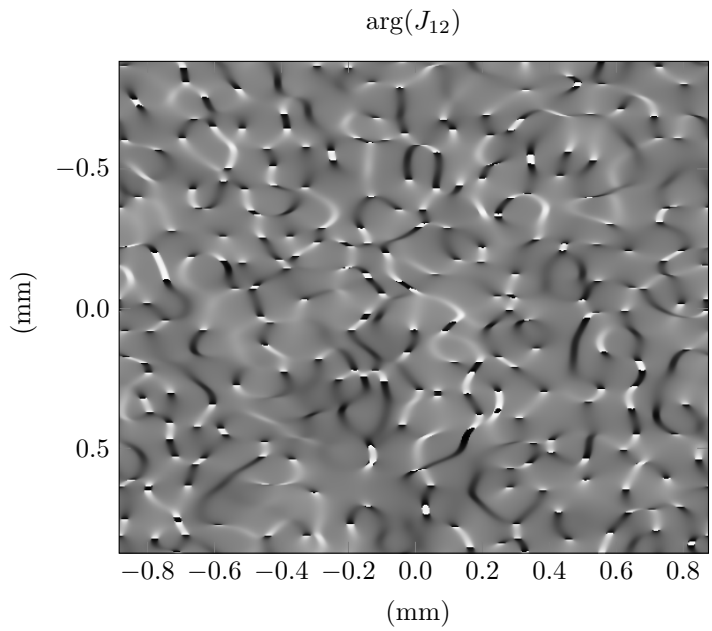

Figure 3.10: *Phase gradient in e_x after one iteration.*

CHAPTER 4

Design parameters

This chapter tries to find analytical expressions for the influence of different parameters observed during simulation.

4.1 Complex coherence factor

In this section we find the analytical solutions to the simulations in section 3.1. The complex coherence factor plays a big role with its relation to the phase error, resolution, and visibility (see sections 4.2, 4.3, and 4.4).

4.1.1 Relationship between Power Spectral Density and Complex Coherence Factor

We wish to find an analytical expression between the power spectral density and mutual coherence factor. By assuming the problem can be solved in one dimension, we write the mutual intensity as if it depends on a position r and a shear Δr

$$J(r, \Delta r) = u(r)u^*(r + \Delta r). \tag{4.1-1}$$

The average mutual intensity will then depend on the shear Δr

$$J(\Delta r) = \left\langle u(r)u^*(r + \Delta r) \right\rangle. \tag{4.1-2}$$

We can then follow the arguments from [9, p.107-108] which looks at the autocorrelation of $u(t)$. First we substitute equation (4.1-2) with $u(r) = u^{(r)}(r) + \mathrm{j}u^{(i)}(r)$, where $u^{(r)}(r)$ is the real part of $u(r)$, and $u^{(i)}(r)$ is the imaginary part of $u(r)$.

$$\begin{aligned} J(\Delta r) &= J^{(r,r)}(\Delta r) + J^{(i,i)}(\Delta r) + \mathrm{j}(J^{(i,r)}(\Delta r) - J^{(r,i)}(\Delta r)) \\ &= 2J^{(r,r)}(\Delta r) + 2\mathrm{j}J^{(i,r)}(\Delta r). \end{aligned} \tag{4.1-3}$$

Then calculate the Fourier transform of $J(\Delta r)$

$$\begin{aligned}\mathscr{G}(\sigma) &\equiv \mathscr{F}[J(\Delta r)] \\ &= 2\mathscr{F}[J^{(r,r)}(\Delta r)] + 2j\mathscr{F}[J^{(i,r)}(\Delta r)] \\ &= 2\mathscr{G}^{(r,r)}(\sigma) + 2\,\mathrm{sgn}(\sigma)\mathscr{G}^{(i,r)}(\sigma) \\ &= \begin{cases} 4\mathscr{G}^{(r,r)}(\sigma) & \sigma > 0 \\ 0 & \sigma < 0 \end{cases}.\end{aligned} \tag{4.1-4}$$

The mutual intensity can then be written

$$J(\Delta r) = \mathscr{F}^{-1}[\mathscr{G}(\sigma)] = \int_0^\infty 4\mathscr{G}^{(r,r)}(\sigma) e^{-\mathrm{j}2\pi\sigma\,\Delta r}\,\mathrm{d}\sigma. \tag{4.1-5}$$

Finally we insert this into the definition of the complex coherence factor from equation (2.3-3) and get

$$\begin{aligned}\mu(\Delta r) &= \frac{J(\Delta r)}{\sqrt{II}} \\ &= \frac{J(\Delta r)}{\sqrt{J(0)J(0)}} \\ &= \frac{\int_0^\infty 4\mathscr{G}^{(r,r)}(\sigma) e^{-\mathrm{j}2\pi\sigma\,\Delta r}\,\mathrm{d}\sigma}{\int_0^\infty 4\mathscr{G}^{(r,r)}(\sigma)\,\mathrm{d}\sigma} \\ &= \int_0^\infty \hat{\mathscr{G}}(\sigma) e^{-\mathrm{j}2\pi\sigma\,\Delta r}\,\mathrm{d}\sigma,\end{aligned} \tag{4.1-6}$$

where $\hat{\mathscr{G}}(\sigma)$ is the *normalized power spectral density*. Now we can expand the solution to the two-dimensional plane where we can write it as a two-dimensional Fourier transform

$$\mu(\Delta r_x, \Delta r_y) = \iint_0^\infty \hat{\mathscr{G}}(\sigma_x, \sigma_y) e^{-\mathrm{j}2\pi(\sigma_x\,\Delta r_x + \sigma_y\,\Delta r_y)}\,\mathrm{d}\sigma_x\,\mathrm{d}\sigma_y. \tag{4.1-7}$$

When $\hat{\mathscr{G}}(\sigma_x, \sigma_y) = \hat{\mathscr{G}}(\sigma_x)\hat{\mathscr{G}}(\sigma_y)$ we can write this as a multiplication in the space-domain

$$\begin{aligned}\mu(\Delta r_x, \Delta r_y) &= \int_0^\infty \hat{\mathscr{G}}(\sigma_x) e^{-\mathrm{j}2\pi\sigma_x\,\Delta r_x)}\,\mathrm{d}\sigma_x \int_0^\infty \hat{\mathscr{G}}(\sigma_y) e^{-\mathrm{j}2\pi(\sigma_y\,\Delta r_y)}\,\mathrm{d}\sigma_y \\ &= \mu_{12}(\Delta r_x)\mu_{12}(\Delta r_y).\end{aligned} \tag{4.1-8}$$

For circular symmetry $\sigma_x^2 + \sigma_y^2 = \sigma_\perp^2$, equation (4.1-7) can be written as the *Hankel transform* [11, p.248]

$$\mu(\Delta r_\perp) = 2\pi \int_0^\infty \hat{\mathscr{G}}(\sigma_\perp)\,\mathrm{J}_0(2\pi\sigma_\perp \Delta r_\perp)\,\mathrm{d}\sigma_\perp, \tag{4.1-9}$$

where J_n is a *Bessel function* of the first kind of order n.

4.1.2 Analytical solution for square bandwidth

As in the numerical model we solve for a speckle pattern with random phase components within the square area spanned by $\Delta\sigma_x^{BW}$ and $\Delta\sigma_y^{BW}$. The condition for equation (4.1-8) is valid and we can calculate the complex coherence individually for e_x and e_y. Along one axis the normalized power spectral density can be written as rectangular in the form

$$\hat{\mathscr{G}}(\sigma) = \frac{1}{\Delta\sigma^{BW}} \operatorname{rect}\left(\frac{\sigma - \bar{\sigma}}{\Delta\sigma^{BW}}\right). \tag{4.1-10}$$

Solving equation (4.1-6) for the normalized power spectral density (4.1-10) gives

$$\begin{aligned}
\mu(\Delta r) &= \int_0^\infty \frac{1}{\Delta\sigma^{BW}} \operatorname{rect}\left(\frac{\sigma - \bar{\sigma}}{\Delta\sigma^{BW}}\right) e^{-\mathrm{j}2\pi\sigma\,\Delta r}\,\mathrm{d}\sigma \\
&= \int_{\bar{\sigma}-\Delta\sigma^{BW}/2}^{\bar{\sigma}+\Delta\sigma^{BW}/2} \frac{1}{\Delta\sigma^{BW}} e^{-\mathrm{j}2\pi\sigma\,\Delta r}\,\mathrm{d}\sigma \\
&= \frac{1}{j2}\left(\frac{e^{\mathrm{j}\pi\,\Delta\sigma^{BW}\,\Delta r} - e^{-\mathrm{j}\pi\,\Delta\sigma^{BW}\,\Delta r}}{\pi\,\Delta\sigma^{BW}\,\Delta r}\right) e^{-\mathrm{j}2\pi\bar{\sigma}\Delta r} \\
&= \operatorname{sinc}(\Delta\sigma^{BW}\,\Delta r) e^{-\mathrm{j}2\pi\bar{\sigma}\Delta r},
\end{aligned} \tag{4.1-11}$$

where $\operatorname{sinc}(x) = \sin(\pi x)/\pi x$. The correlation along each axis e_x and e_y thus depend on speckle bandwidth and shear length by

$$\left|\mu_{12}(\Delta r)\right| = \left|\operatorname{sinc}(\Delta\sigma^{BW}\,\Delta r)\right|. \tag{4.1-12}$$

Using equation (4.1-8) the correlation in the whole plane is

$$\left|\mu_{12}(\Delta r_x, \Delta r_y)\right| = \left|\operatorname{sinc}(\Delta\sigma_x^{BW}\,\Delta r_x)\operatorname{sinc}(\Delta\sigma_y^{BW}\,\Delta r_y)\right|. \tag{4.1-13}$$

A comparison between the numerical solution described in section 3.1 and the analytical expression described here can be seen in figure 4.1. The simulation results are cut out along e_x from the two dimensional autocorrelation matrix seen in figure 3.1.

4.1.3 Analytical solution for circular bandwidth

For a circular bandwidth the spatial frequencies are contained inside a circular area with the radius $a = \Delta\sigma_\perp^{BW}/2$, the normalized power spectral density in the plane can be written

$$\hat{\mathscr{G}}(\sigma_\perp) = \frac{1}{\pi a^2} \operatorname{rect}\left(\frac{\sigma_\perp}{2a}\right), \tag{4.1-14}$$

where $\sigma_\perp = \sqrt{\sigma_x^2 + \sigma_y^2}$. The function clearly has circular symmetry and thus fulfills the condition for the Hankel transform (4.1-9). [11, p.249] lists the Hankel transform

$$\mathscr{F}\left[\operatorname{rect}\left(\frac{\sigma_\perp}{2a}\right)\right] = \frac{a\,\mathrm{J}_1(2\pi a r_\perp)}{r_\perp}. \tag{4.1-15}$$

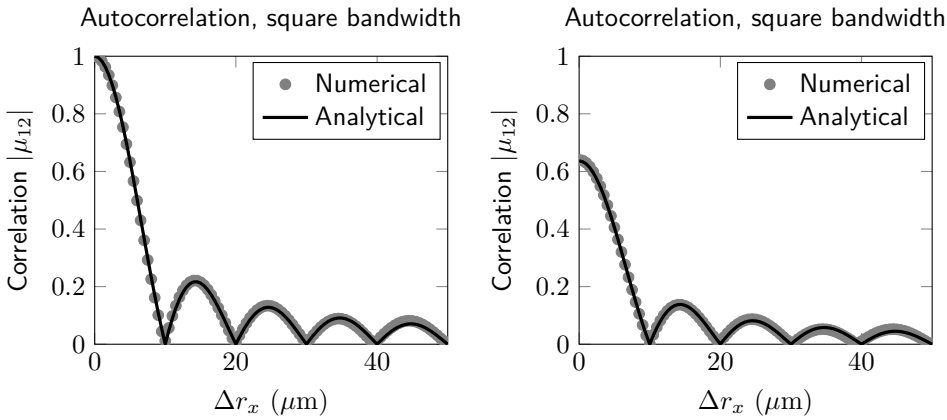

(a) $\Delta r_y = 0\mu m$ **(b)** $\Delta r_y = 10\mu m$

Figure 4.1: *The autocorrelation of square bandwidth along e_x for two different shears in e_y. The maximum spatial frequency of the speckle pattern is $\Delta\sigma_x^{BW} = \Delta\sigma_y^{BW} = 1/(10\mu m)$. The numerical value is calculated on a 2048x2048 grid with the pixel pitch $d = 0.5\mu m$.*

Applying it to equation (4.1-14) gives us the complex coherence factor for a circular bandwidth as

$$\mu_{12}(\Delta r_\perp) = \frac{\mathrm{J}_1(2\pi a r_\perp)}{\pi a r_\perp}, \tag{4.1-16}$$

and the correlation

$$\left|\mu_{12}(\Delta r_\perp)\right| = \left|\frac{\mathrm{J}_1(2\pi a r_\perp)}{\pi a r_\perp}\right|. \tag{4.1-17}$$

A comparison between the numerical solution described in section 3.1 and the analytical expression described here can be seen in figure 4.2. The simulation results are cut out along e_x from the two dimensional autocorrelation matrix seen in figure 3.2.

4.2 Phase error

This section looks at what relation the degree of spatial and temporal coherence have in relation to the phase error. The spatial coherence is related to the phase error by the correlation examined in the previous section. The temporal coherence is related to the phase error by its averaging effect over time, as seen in subsection 4.2.1.

The relation between the phase error and correlation is given by [12] and shown here in equation (4.2-1) to (4.2-4) The Phase error distribution as a function of the correlation is given as

$$p_{\phi_e}(\phi_e) = \frac{1-|\mu|^2}{2\pi}(1-\beta^2)^{-\frac{3}{2}}\left(\beta\arcsin\beta + \frac{\pi\beta}{2} + \sqrt{1-\beta^2}\right), \tag{4.2-1}$$

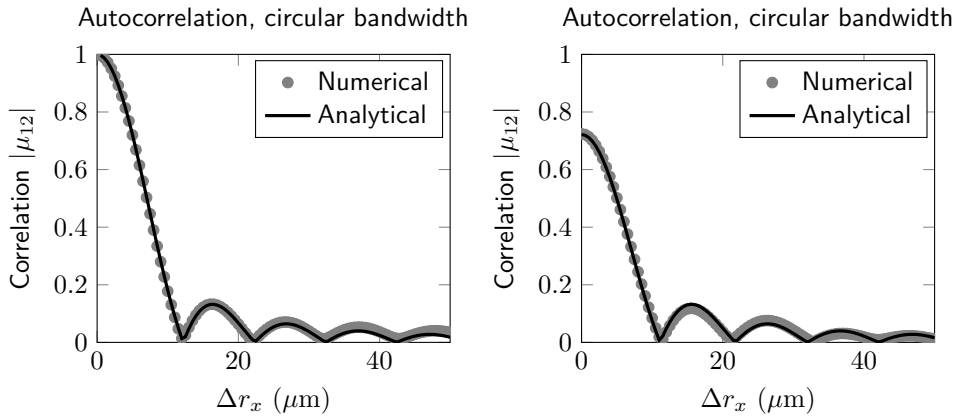

(a) $\Delta r_y = 0\mu m$ **(b)** $\Delta r_y = 10\mu m$

Figure 4.2: *The autocorrelation of circular bandwidth along e_x for two different shears in e_y. The maximum spatial frequency of the speckle pattern is $\Delta\sigma_x^{BW} = \Delta\sigma_y^{BW} = 1/(10\mu m)$. The numerical value is calculated on a 2048x2048 grid with the pixel pitch $d = 0.5\mu m$.*

where

$$\beta = |\mu| \cos(\phi_e). \tag{4.2-2}$$

The standard deviation of the phase error is given as

$$\mathrm{std}(\phi_e) = \sqrt{\frac{\pi^2}{3} - \pi \arcsin|\mu| + \arcsin^2|\mu| - \frac{1}{2}\sum_{n=1}^{\infty}\frac{\mu^{2n}}{n^2}}, \tag{4.2-3}$$

which has the approximation

$$\mathrm{std}(\phi_e) \approx (\pi/\sqrt{3})(1-|\mu|)^{0.42}. \tag{4.2-4}$$

The standard deviation given in equation (4.2-3) and (4.2-4) is the standard deviation of the phase error for fully temporally coherent light. In which case we only have the contributions of a single speckle pattern and no temporal averaging as described by equation (2.3-2) has taken place. These values of the standard deviation of the phase error correspond to the starting values in figure 4.3.

4.2.1 Phasor sum

It should be possible to get an expression for the standard deviation of the phasor sum in equation (2.3-2) (see [13]). We however are content with showing a numerical example by summing up uncorrelated speckle patterns. See figure 4.3. As mentioned in section 2.3, the sum of the random phasors distributed around zero will go towards a real positive number. With other words, the phase error will go towards zero. For coherent light $|\mu| = 1$, the phase error is zero, and therefore the standard deviation of the phase error is also zero. For incoherent light $|\mu| = 0$, the phase error is uniformly

distributed between $-\pi$ and π (see figure 2.2). Such a distribution has the standard deviation $\pi/\sqrt{3}$ and a simulation of it would only show a random walk around this standard deviation. For a large number of iterations we can see that the standard deviation approaches

$$x/\sqrt{N}, \tag{4.2-5}$$

where N is the number of iterations or uncorrelated speckle patterns, and x is not directly given by equation (4.2-3) and (4.2-4), but is some value dependent on the distribution function (4.2-1). As reference, $1/\sqrt{N}$ is plotted among the phasor sums in figure 4.3.

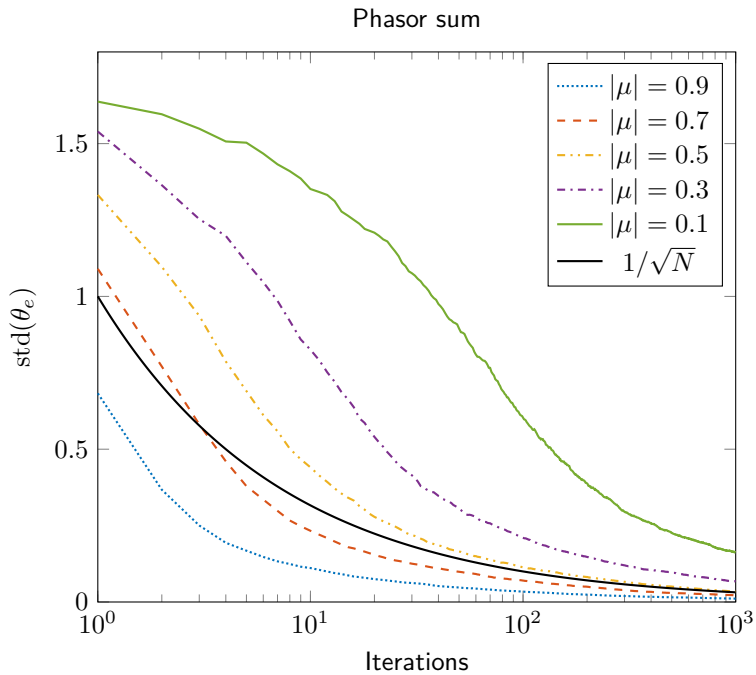

Figure 4.3: *Example of a phasor sum going towards a real positive value. The y-axis show the standard deviation of the phase error. The x-axis shows the number of iterations and is logarithmic. The lines differ in terms of what correlation the speckle pattern generated each iteration has.* $1/\sqrt{N}$ *is plotted for reference where* N *is the number of iterations.*

4.3 Numerical Aperture

This section looks at how the numerical aperture and degree of spatial coherence relates to what spatial frequencies in the object are possible to recreate in the image plane.

The interaction between the source light and the object plane can be described as a multiplication between the source lights complex wave function u_s and a complex object u_{obj}

$$u_0(\boldsymbol{r}) = u_s(\boldsymbol{r})u_{obj}(\boldsymbol{r}). \tag{4.3-1}$$

This operation corresponds to a convolution in the frequency domain

$$U_0(\boldsymbol{\sigma}) = U_s(\boldsymbol{\sigma}) * U^*_{obj}(-\boldsymbol{\sigma}). \tag{4.3-2}$$

For the case of fully spatially coherent source light, u_s is constant over the plane and U_s is described solely by its center frequency. In this case the frequencies limited by the aperture directly correspond to the frequencies in the object

$$NA_0 \equiv \max(s_{\perp,0}) = \max(s_{\perp,obj}). \tag{4.3-3}$$

If the source light is not completely spatially coherent this relation no longer holds true. Each individual frequency in the object will through the convolution with the source light get spread out in the shape of the speckle frequencies. If the spread of a frequency is fully contained inside the aperture it will contribute with its full amplitude to the image. If the spread of a frequency is completely outside the aperture, it will of course not contribute to the image at all. For the cases in-between the amplitude of the frequency is lowered and thus its gradient. It is interesting to note that it is possible to see frequency components in the object that is higher than those the aperture lets through. Increasing the speckle bandwidth makes frequency components larger than the aperture size more visible and those smaller than the aperture size less visible.

4.4 Visibility

To motivate a definition of the fringe visibility between three interfering wave fronts we start from the definition for fringe visibility between two interfering wavefronts. The total intensity from two interfering wave functions u_1 and u_2 can using equation (2.3-3) be written as

$$\begin{aligned} I &= \left\langle u(\boldsymbol{r})u^*(\boldsymbol{r}) \right\rangle \\ &= \left\langle \left(u_1(\boldsymbol{r}) + u_2(\boldsymbol{r})\right)\left(u_1(\boldsymbol{r}) + u_2(\boldsymbol{r})\right)^* \right\rangle \\ &= J_{11} + J_{22} + J_{12} + J^*_{12} \\ &= J_{11} + J_{22} + 2|J_{12}|\cos(\arg(J_{12})) \\ &= J_{11} + J_{22} + 2\sqrt{J_{11}J_{22}}|\mu_{12}|\cos(\arg(J_{12})) \\ &= I_1 + I_2 + 2\sqrt{I_1 I_2}|\mu_{12}|\cos(\arg(J_{12})). \end{aligned} \tag{4.4-1}$$

where we make the simplification that the intensity of each component $I_1 = J_{11}$ and $I_2 = J_{22}$ is constant. In the interference between two wave functions the *visibility* first defined by Michelson is

$$\begin{aligned} \mathscr{V} &\equiv \frac{\max(I) - \min(I)}{\max(I) + \min(I)} \\ &= \frac{2\sqrt{I_1 I_2}}{I_1 + I_2}|\mu_{12}|. \end{aligned} \tag{4.4-2}$$

From its definition, the visibility gives a measure of how much outside disturbances affect the image quality. Indirectly, through its relation with the complex coherence factor it also gives a measure of the physical disturbances from speckles. For $I_1 = I_2$ it is worth noting that equation 4.4-2 can be simplified to

$$\mathscr{V} = |\mu_{12}|, \tag{4.4-3}$$

which it is easy to see is the maximum visibility. If the phase difference between u_1 and u_2 is $\arg(J_{12}) = \phi(r)$, a frequency shift of u_2 by $\Delta\sigma$ as in our imaging system, gives

$$\arg(J_{12}) = 2\pi\,\Delta\sigma r + \phi(r). \tag{4.4-4}$$

Inserting equation (4.4-2) and (4.4-4) into (4.4-1) results in

$$I(r) = (I_1 + I_2)\left(1 + \mathscr{V}\cos\left(2\pi\,\Delta\sigma r + \phi(r)\right)\right). \tag{4.4-5}$$

In the intensity pattern there will thus be fringes with amplitude $(I_1 + I_2)\mathscr{V}$ around $I_1 + I_2$ with the period $1/\,\Delta\sigma$. Because of variations in the phase it's hard to measure the visibility experimentally directly in the spatial domain. Instead we use the Fourier transform to look at the problem in the spatial frequency domain. The *Modulation Theorem* [11, p. 182] gives the Fourier transform of equation (4.4-5)

$$\begin{aligned}
\tilde{I}(\sigma) &= \mathscr{F}[I(r)] \\
&= (I_1 + I_2)\left(\delta(\sigma) + \frac{1}{2}\mathscr{V}\left(\delta(\sigma - \Delta\sigma) + \delta(\sigma + \Delta\sigma)\right)\right) \\
&= \begin{cases} I_1 + I_2 & \sigma = 0 \\ \frac{1}{2}(I_1 + I_2)\mathscr{V} & \sigma = \pm\,\Delta\sigma\,, \\ 0 & \text{otherwise} \end{cases}
\end{aligned} \tag{4.4-6}$$

where we made the simplification $\phi(r) = 0$ with the motivation that it is generally not periodic, and for our system $\phi(r) \leq \Delta\sigma$ as the interference lobes would otherwise overlap (see section 2.2). Solving equation (4.4-6) for the visibility $\mathscr{V}$ yields

$$\mathscr{V} = \frac{2\tilde{I}(\pm\,\Delta\sigma)}{\tilde{I}(0)} \tag{4.4-7}$$

A comparison between using equation (4.4-7) to get the visibility from a simulation run and calculating it analytically with equation (4.4-6) can be seen in figure 4.4.

For three components the intensity can, similar to the two component system in equation 4.4-8 be written

$$\begin{aligned}
I &= \left\langle (u_1(\boldsymbol{r}) + u_2(\boldsymbol{r}) + u_3(\boldsymbol{r}))(u_1(\boldsymbol{r}) + u_2(\boldsymbol{r}) + u_3(\boldsymbol{r}))^* \right\rangle \\
&= J_{11} + J_{22} + J_{33} + J_{12} + J_{12}^* + J_{13} + J_{13}^* + J_{23} + J_{23}^* \\
&= I_1 + I_2 + I_3 + 2\sqrt{I_1 I_2}|\mu_{12}|\cos(\arg(J_{12})) \\
&\qquad + 2\sqrt{I_1 I_3}|\mu_{13}|\cos(\arg(J_{13})) \\
&\qquad + 2\sqrt{I_2 I_3}|\mu_{23}|\cos(\arg(J_{23}))
\end{aligned} \tag{4.4-8}$$

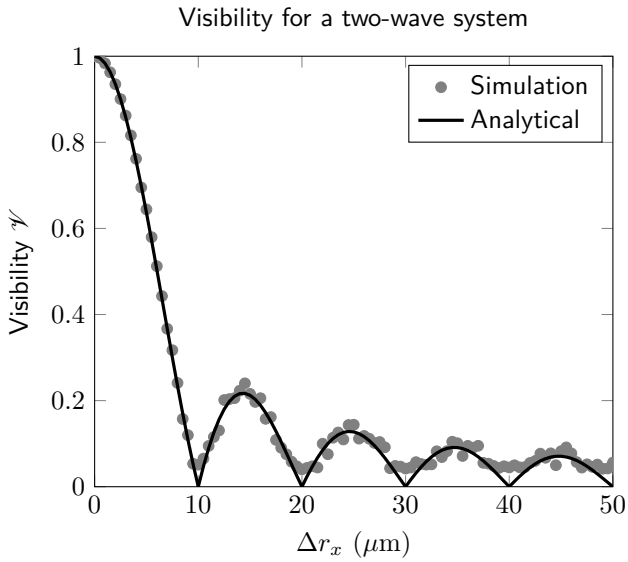

Figure 4.4: *The visibility with only two wave components for a given shear. The bandwidth of the light source is square with maximum spatial frequencies* $\Delta\sigma_x^{BW} = \Delta\sigma_y^{BW} = 1/(10\mu m)$ *and the intensity of the components are equal* $I_1 = I_2$.

For simplicity, u_2 and u_3 are shifted in frequency from u_1 in perpendicular directions (see figure 1.2). The arguments in (4.4-8) can then be written

$$\arg(J_{12}) = 2\pi\,\Delta\sigma_x r_x + \phi_{12}(r_x, r_y), \tag{4.4-9}$$

$$\arg(J_{13}) = 2\pi\,\Delta\sigma_y r_y + \phi_{13}(r_x, r_y), \tag{4.4-10}$$

$$\arg(J_{23}) = \arg(J_{13}) - \arg(J_{12}), \tag{4.4-11}$$

and the Fourier transform

$$\begin{aligned}
\tilde{I}(\sigma_x, \sigma_y) &= \mathscr{F}[I(r_x, r_y)] \\
&= (I_1 + I_2 + I_3)\delta^2(\sigma_x, \sigma_y) \\
&+ \sqrt{I_1 I_2}|\mu_{12}|\left(\delta^2(\sigma_x - \Delta\sigma_x, \sigma_y) + \delta^2(\sigma_x + \Delta\sigma_x, \sigma_y)\right) \\
&+ \sqrt{I_1 I_3}|\mu_{13}|\left(\delta^2(\sigma_x, \sigma_y - \Delta\sigma_y) + \delta^2(\sigma_x, \sigma_y + \Delta\sigma_y)\right) \\
&+ \sqrt{I_2 I_3}|\mu_{23}|\left(\delta^2(\sigma_x - \Delta\sigma_x, \sigma_y + \Delta\sigma_y) + \delta^2(\sigma_x + \Delta\sigma_x, \sigma_y - \Delta\sigma_y)\right) \\
&= \begin{cases}
I_1 + I_2 + I_3, & (\sigma_x, \sigma_y) = (0, 0) \\
\sqrt{I_1 I_2}|\mu_{12}| & (\sigma_x, \sigma_y) = \pm(\Delta\sigma_x, 0) \\
\sqrt{I_1 I_3}|\mu_{13}| & (\sigma_x, \sigma_y) = \pm(0, \Delta\sigma_y) \\
\sqrt{I_2 I_3}|\mu_{23}| & (\sigma_x, \sigma_y) = \pm(\Delta\sigma_x, -\Delta\sigma_y) \\
0 & \text{otherwise}
\end{cases},
\end{aligned} \tag{4.4-12}$$

where the simplification $\phi_{12}(r_x, r_y) = \phi_{13}(r_x, r_y) = 0$ is made with the same motivation as for equation (4.4-6).

In the two component system we defined the visibility according to equation (4.4-2). For the three component system that definition does not give us the information we want. It gives a single value for the whole system, while our fringe pattern contains three individually interesting frequencies. Therefore, we define the visibility of a certain frequency as its amplitude relative to the mean

$$\mathscr{V}(\sigma_x, \sigma_y) \equiv \frac{2\tilde{I}(\sigma_x, \sigma_y)}{\tilde{I}(0,0)}. \tag{4.4-13}$$

Inserting equation (4.4-12) into (4.4-13) yields

$$\mathscr{V}_{ij} = \frac{2\sqrt{I_i I_j}}{I_1 + I_2 + I_3} \left|\mu_{ij}\right|, \tag{4.4-14}$$

where $ij = \{12, 13, 23\}$ and corresponds to the visibility of each of the three frequencies visible in the fringe pattern. For $I_3 = 0$ we get the definition of the two component visibility defined in equation (4.4-2). A comparison between using equation (4.4-13) to get the visibility from a simulation and calculating it analytically with equation (4.4-14) can be seen in figure 4.5.

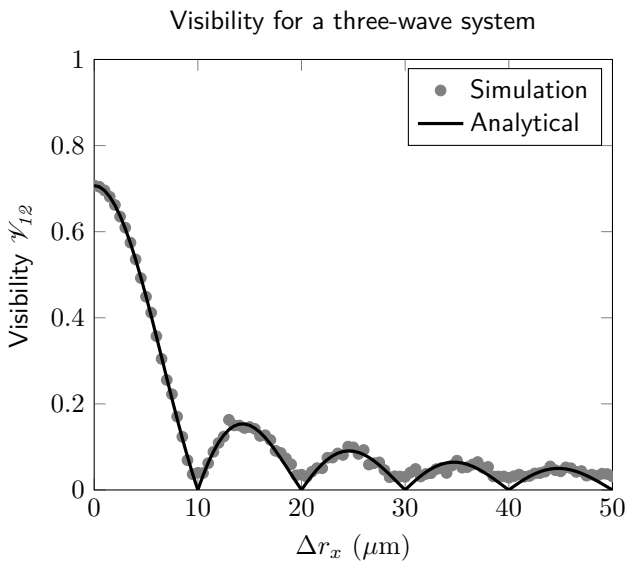

Figure 4.5: *The visibility $\mathscr{V}_{12}$ with three wave components for a given shear of U_2. The bandwidth of the light source is square with maximum spatial frequencies $\Delta\sigma_x^{BW} = \Delta\sigma_y^{BW} = 1/(10\mu m)$ and the components intensities relate by $I_1 = 2I_2 = 2I_3$*

For $I_1 = I_2 = I_3$ the visibility simplifies to

$$\mathscr{V}_{ij} = \frac{2}{3}|\mu_{ij}|. \tag{4.4-15}$$

It is however of more interest to maximize the visibility when $I_2 = I_3 = xI_1$ where x is the positive scalar $x = I_2/I_1 = I_3/I_1$. This is a probable setup when you have a reference with intensity I_1, two referents with intensities I_2 and I_3, and want two equally visible mutual intensities J_{12} and J_{13} from the interference. With this condition one can write the visibilities

$$\mathscr{V}_{12}(x) = \frac{2\sqrt{x}}{1+2x}|\mu_{12}|, \tag{4.4-16}$$

$$\mathscr{V}_{13}(x) = \frac{2\sqrt{x}}{1+2x}|\mu_{13}|, \tag{4.4-17}$$

$$\mathscr{V}_{23}(x) = \frac{2x}{1+2x}|\mu_{23}|. \tag{4.4-18}$$

These functions are plotted in figure 4.6.

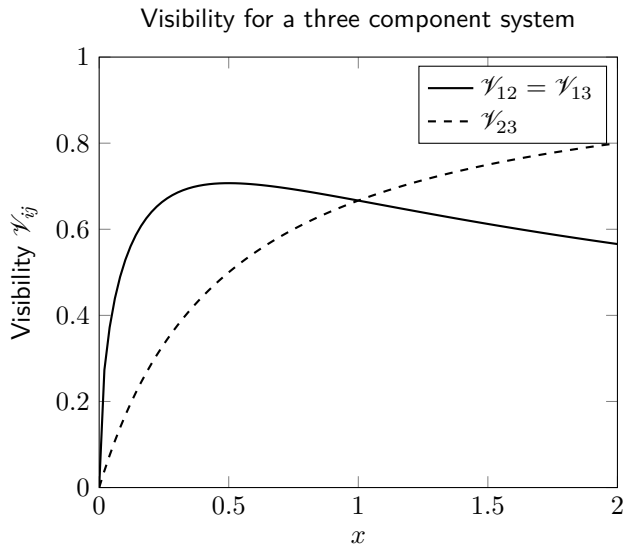

Figure 4.6: *The visibilities when $I_2 = I_3 = xI_1$ and $|\mu_{ij}| = 1$. Illustrates the visibilities dependence on the relative intensity.*

To find the maximum visibility $\mathscr{V}_{12}$ and $\mathscr{V}_{13}$ we take the derivative

$$\begin{aligned} \frac{\mathrm{d}\mathscr{V}_{12}(x)}{\mathrm{d}x} &= \left(\frac{1}{\sqrt{x}(1+2x)} - \frac{4\sqrt{x}}{(1+2x)^2}\right)|\mu_{12}| = 0 \\ &\Rightarrow \\ x &= \frac{1}{2}, \end{aligned} \tag{4.4-19}$$

giving the visibilities

$$\mathscr{V}_{12}(x=0.5) = \frac{1}{\sqrt{2}}|\mu_{12}|, \tag{4.4-20}$$

$$\mathscr{V}_{13}(x=0.5)=\frac{1}{\sqrt{2}}|\mu_{13}|, \tag{4.4-21}$$

$$\mathscr{V}_{23}(x=0.5)=\frac{1}{2}|\mu_{23}|. \tag{4.4-22}$$

4.5 Impact of defocus

This section looks at the effects on the system when introducing a defocus in the image plane. In this section we write the shift theorem in the form

$$e^{-\mathrm{j}k\boldsymbol{r}\cdot\boldsymbol{s}}, \tag{4.5-1}$$

where k is the wavenumber, $\boldsymbol{s}=\lambda\boldsymbol{\sigma}$, $|\boldsymbol{s}|=1$ and $\boldsymbol{\sigma}$ is the spatial frequencies of the wave. We define the phase term of the translational operator

$$\Psi\equiv k\boldsymbol{r}\cdot\boldsymbol{s}=k(r_\perp s_\perp+r_z s_z). \tag{4.5-2}$$

The plane wave propagating in the direction e_z has the group velocity $\frac{\partial\Psi}{k\partial s_\perp}=0$ in the direction of the plane. This gives the condition

$$\begin{aligned}\frac{\partial\Psi}{k\partial s_\perp}&=\frac{\partial(r_\perp s_\perp+r_z\sqrt{1-s_\perp^2})}{\partial s_\perp}\\&=r_\perp-\frac{s_\perp}{\sqrt{1-s_\perp^2}}\\&=r_\perp-\frac{s_\perp}{s_z}r_z=0\\&\Rightarrow r_\perp s_z=r_z s_\perp.\end{aligned} \tag{4.5-3}$$

The spatial frequencies is defined by the Fourier transform of the complex wave

$$\mathscr{F}[u(r_x,r_y)]=U(\sigma_x,\sigma_y)=U(s_x,s_y). \tag{4.5-4}$$

Rewriting it by the coordinate transform $r_\perp=\sqrt{r_x^2+r_y^2}$ we have

$$\mathscr{F}[u(r_\perp)]=U(\sigma_\perp)=U(s_\perp)=U(s_\perp). \tag{4.5-5}$$

The waves going through the optical system can be described as getting a lateral shear, a shift in frequency followed by a possible defocus. We start by applying a lateral shear

$$U_{shear}(s_\perp)=U(s_\perp)e^{-\mathrm{j}kr_\perp s_\perp}. \tag{4.5-6}$$

Then we add a frequency shift

$$\begin{aligned}U_{shear,shift}(s_\perp)&=U_{shear}(s_\perp-\Delta s_\perp)\\&=U(s_\perp-\Delta s_\perp)e^{-\mathrm{j}kr_\perp(s_\perp-\Delta s_\perp)}.\end{aligned} \tag{4.5-7}$$

The last step is to apply a defocus, which is simply a translation along the propagation direction z

$$\begin{aligned}U_{shear,shift,diffract}(s_\perp)&=U_{shear,shift}(s_\perp)e^{-\mathrm{j}kr_z s_z}\\&=U_{shear,shift}(s_\perp)e^{-\mathrm{j}kr_z\sqrt{1-s_\perp^2}}\\&=U(s_\perp-\Delta s_\perp)e^{-\mathrm{j}k\left(r_\perp(s_\perp-\Delta s_\perp)+r_z\sqrt{1-s_\perp^2}\right)},\end{aligned} \tag{4.5-8}$$

where we used $s_z = \sqrt{1 - s_\perp^2}$.

From equation (4.5-8) one can see that defocus results in an additional shear, and a phase offset, both depending on the frequency shift $\Delta s_\perp$. For the additional shear, we can see that it is independent of any earlier applied shear. From the perspective of the reference wave, the additional shear of the referent depend on the distance between the reference and referents center frequencies. Using equation 4.5-3, separating reference and referents center frequencies by $\Delta s_\perp$, the referent wave will under the influence of a defocus $r_z = \Delta r_z$ shear by

$$\Delta r_\perp = \frac{\Delta s_\perp}{\Delta s_z} \Delta r_z, \tag{4.5-9}$$

where $\Delta s_z = \sqrt{1 - (\Delta s_\perp)^2}$. Because of the magnification in the imaging system we can write this as

$$\Delta r_\perp = \frac{\Delta s_\perp}{\Delta s_z} \frac{\Delta z_2}{m}. \tag{4.5-10}$$

As for the phase shift in equation 4.5-8 it can be written

$$\phi_{offset} = k \, \Delta s_z \, \Delta r_z = k \, \Delta s_z \, \Delta z_2. \tag{4.5-11}$$

This offset can be eliminated by making sure you have the same offset for the reference as the referent. For a reference separated in frequency from two referents by Δs in e_x and e_y respectively, we should have the frequency shifts

$$\begin{aligned} \Delta \boldsymbol{s}_1 &= (-\Delta s/2, -\Delta s/2) \\ \Delta \boldsymbol{s}_2 &= (\Delta s/2, -\Delta s/2) \\ \Delta \boldsymbol{s}_3 &= (-\Delta s/2, \Delta s/2), \end{aligned} \tag{4.5-12}$$

where $\Delta \boldsymbol{s}_1$ is the reference shift, $\Delta \boldsymbol{s}_2$ is the referent shifted in e_x, and $\Delta \boldsymbol{s}_3$ is the referent shifted in e_y. This is of course assuming we are shifting in perpendicular directions as in the illustration shows in figure 1.2. For a circular aperture it is possible to pack the spatial frequency lobes in the total intensity in a tighter pattern by not shifting the spatial frequencies in perpendicular directions. The optimal pattern in the case for a circular aperture for using as little spatial frequency space as possible would be to shift the spatial frequencies into a equilateral triangle.

CHAPTER 5

Experiment

An experiment is conducted to validate the simulation and analytical models of the system parameters.

5.1 Experimental setup

The simplest experimental setup possible is used to validate the simulation and analytical model. Instead of two referents only one referent is used, and we will not shear the referent using a prism in the aperture plane, but let it be introduced through a defocus as shown in section 4.5, or through intentional misalignment of mirrors.

An illustration of the optical system can be seen in figure 5.1. It is set up as a 4-f system with a limiting aperture in the Fourier plane (see section 2.4). Between the aperture and the second lens the wave is split by a beam-splitter, the split waves are reflected back using two perpendicular mirrors and are through this operation shifted in frequency. In a 4-f system there is a well defined Fourier plane where the entrance pupil has effectively performed a Fourier transform of the wavefront [10]. This point is for our system a distance f_1 away from the entrance pupil, which is where we place the aperture to control our maximum spatial frequency. The frequency is shifted by a similar principle as the aperture limits the maximum spatial frequency.

As a lateral translation of light through reflection by two mirrors is independent of when it is performed, we can cause the spatial frequency shift by such a translation at any point between our two lenses. The frequency shift $\Delta\sigma$ will not be affected by at which point between the two lenses we perform it. At least not as long as one keeps the angle of incidence of the light at zero, such that the center of the wavefront is positioned at the center of the system. The mirrors mimic so called corner-cubes and both pairs of mirrors are placed in the same formation. Looking at the arrows drawn in figure 5.1 and thinking about how they interact when hitting the beam splitter again, one can see that the result is identical frequency shifts in opposite directions.

The wavefronts lose more intensity as they pass through the beam-splitter again,

but because we need some integration time the loss in intensity can be seen as beneficial. The main reason for the beam-splitter and mirrors to be in this configuration is because it allows the frequency shift to be quite small without having very small mirrors or huge lenses. The focal length of the exit pupil F_2 has to be of reasonable length to fit all the components between it and the aperture. In the end, $f_2 = 250$ mm was chosen. For the focal length of the entrance pupil F_1 some considerations for filling up the whole sensor had to be made. $f_1 = 120$ mm was chosen giving the magnification $m \approx 2.1$.

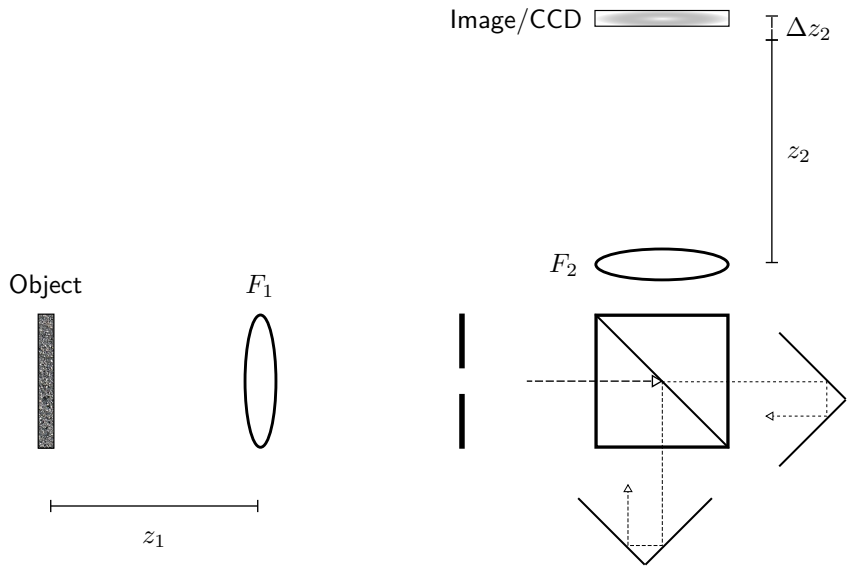

Figure 5.1: *Illustration of the experimental setup from the object to the CCD-camera. The light-source enter from the bottom left where it hits the object. Measured in optical path the aperture in the center of the image is located z_1 from f_1 and z_2 from f_2.*

An illustration of the setup for controlling the light source can be seen in Figure 5.2. The beam of a 1 mW, 633 nm, Helium-Neon laser was expanded by a Galilean beam expander. The beam could then be limited with an aperture to desired width before hitting the diffuser. The speckle size could then be controlled by either changing the beam width w with this aperture or changing the distance L between the diffuser and object. To get uncorrelated speckle patterns the diffuser was mounted to an electrical engine with the constant speed of 92.5 rpm. The radius R between the center of rotation of the diffuser and the beam, the beam width, the distance between diffuser and object, the rotational speed of the diffuser, and the exposure time can give an estimate of the total number of uncorrelated speckle patterns.

Photos of the setup can be seen in figure 5.3 and figure 5.4. One of the practical difficulties was to align it properly. Small changes in the angle of incidence had a big impact on the frequency shift. The easiest way to go about it was to do the aligning using the laser without the diffuser, and during measurements make sure that the angle of incidence of the light is zero and only do very small adjustments to the system.

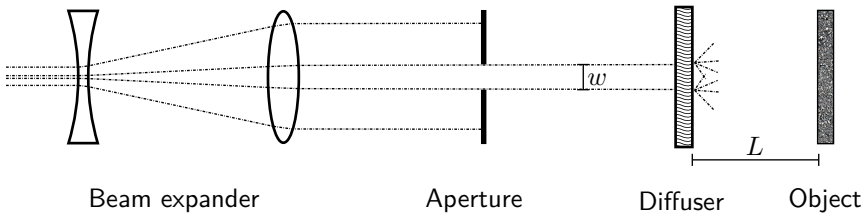

Figure 5.2: *Illustration of how the source light is set up. The beam width w and diffuser to object length L are marked out.*

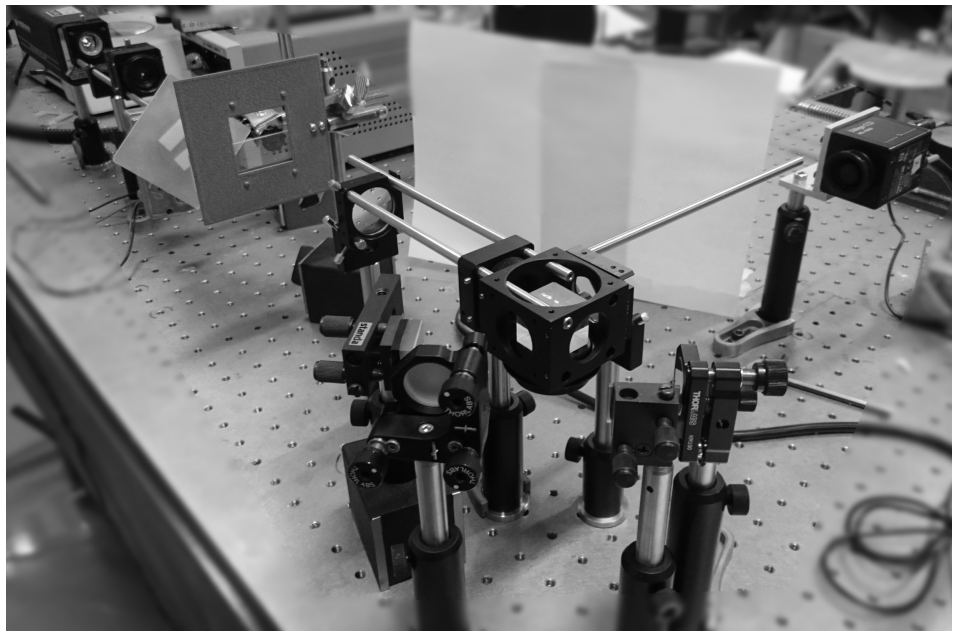

Figure 5.3: *Picture of the experimental setup used for the experiments. Compare to the illustration in figure 5.1.*

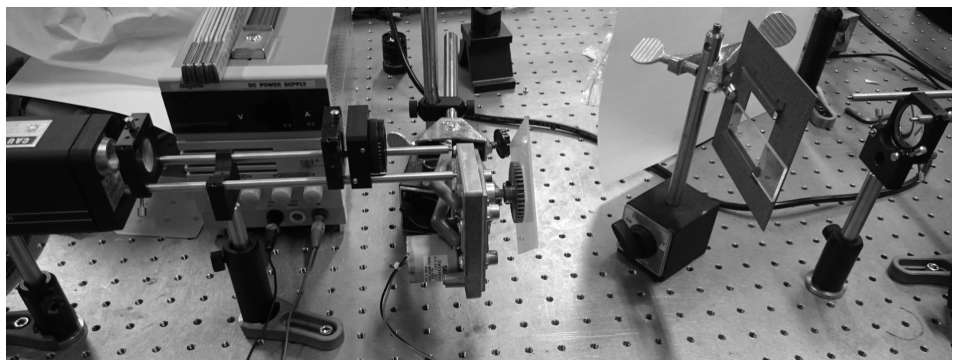

Figure 5.4: *Picture of the how the light source is set up. Compare to the illustration in figure 5.2.*

5.2 Example image

This subsection shows the information extracted from an image. The specific image was chosen on the basis that it looked the most interesting and the phase gradients generally stay below $\pm\pi$. Images with larger shear does however make sharp edges more visible as the gradient marking it gets wider. The object is some water trapped between two glass plates. The shear was achieved by a defocus of 2 mm. Full list of parameters used can be found in table 5.1.

Parameters	
Wavelength λ	633 nm
Entrance pupil f_1	120 mm
Exit pupil f_2	250 mm
Beam width w	1.5 mm
Diffuser to object L	160 mm
Diffuser radius	35 mm
Diffuser speed	92.5 rpm
Exposure time	200 ms
Defocus Δz	2 mm
Limiting aperture	5 mm
Camera resolution	2048x2448 px
Pixel pitch	3.45x3.45 µm

Table 5.1: *Parameters used for the example image*

Figure 5.5 shows the camera output. The intensity for this image was quite low with a mean intensity of 42 out of 255 (8-bit). Its contrast has therefore been adjusted to make it more visible. In figure 5.6 one can see the spatial frequency domain of the image.

Two different ways to view the amplitudes can be seen in figure 5.7 and 5.8. Only the second image showing the absolute value of the mutual intensities is a product of interference. The first picture showing the sum of intensities corresponds to what you would get with incoherent light. The main source of differences in amplitude comes from scattering at sharp incidence angles of the water.

Figure 5.9 and 5.10 shows the phase gradient. In the first image one can see a spherical curvature of the phase. This contribution is not due to a phase gradient in the object, but due to a slight difference in optical path through the imaging system for the split wavefronts. The other picture of the phase gradient has this contribution filtered away with an averaging filter.

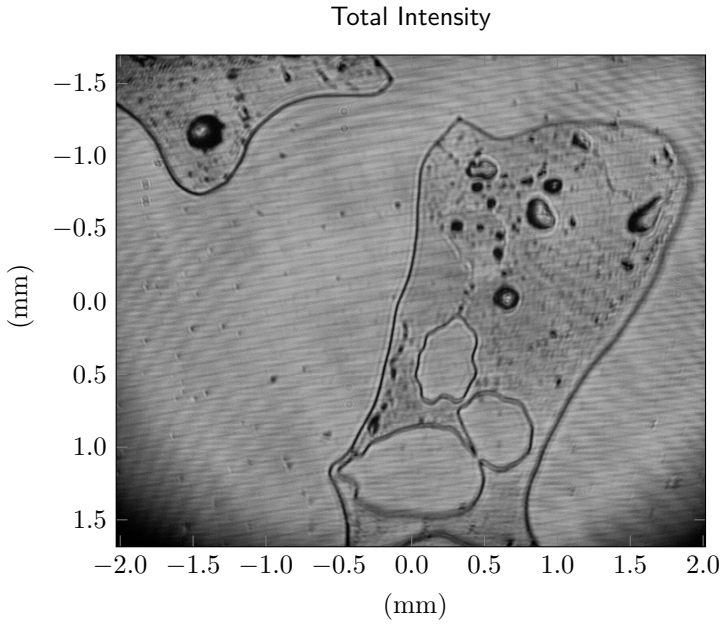

Figure 5.5: *The camera output. 8-bit greyscale, 2048x2448 px.*

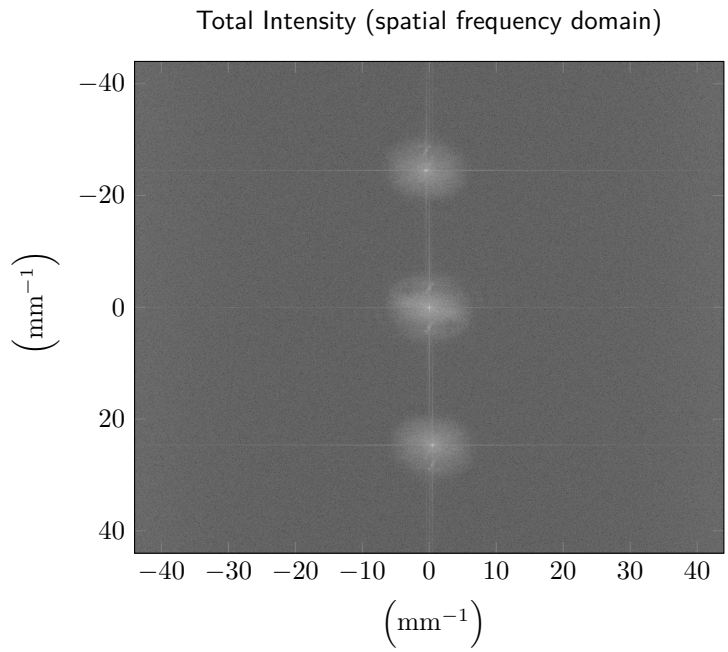

Figure 5.6: Fourier transform of the camera output in figure 5.5. The image shows the logharitmic absolute values.

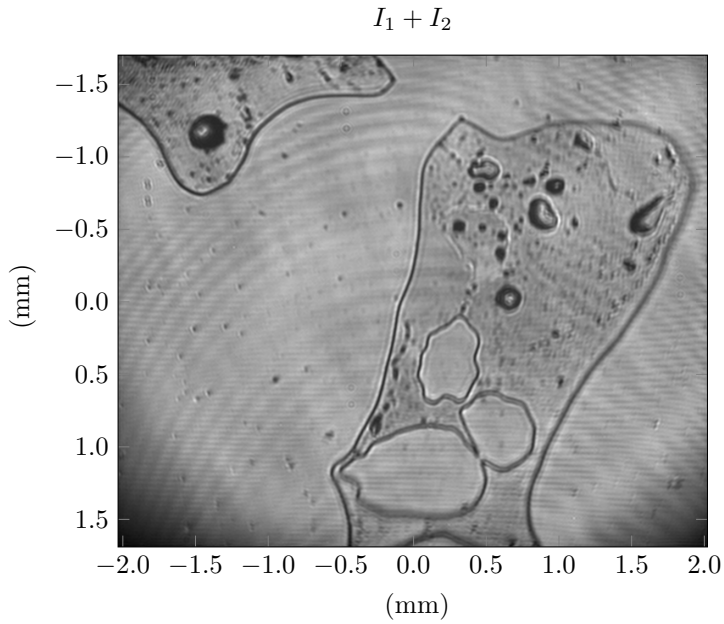

Figure 5.7: *Sum of the intensities. Extracted by filtering out all but the center lobe in figure 5.6.*

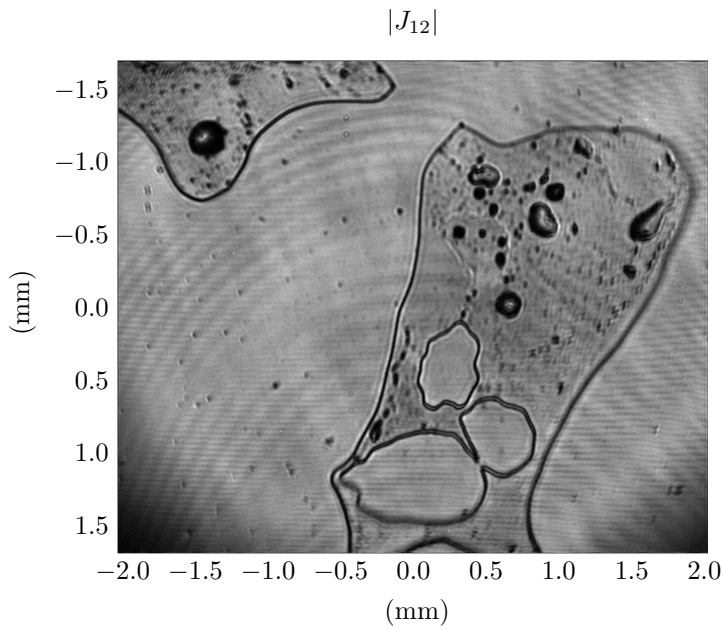

Figure 5.8: *Absolute value of Mutual intensity. Extracted by filtering out all but the bottom lobe in figure 5.6 and taking the absolute value.*

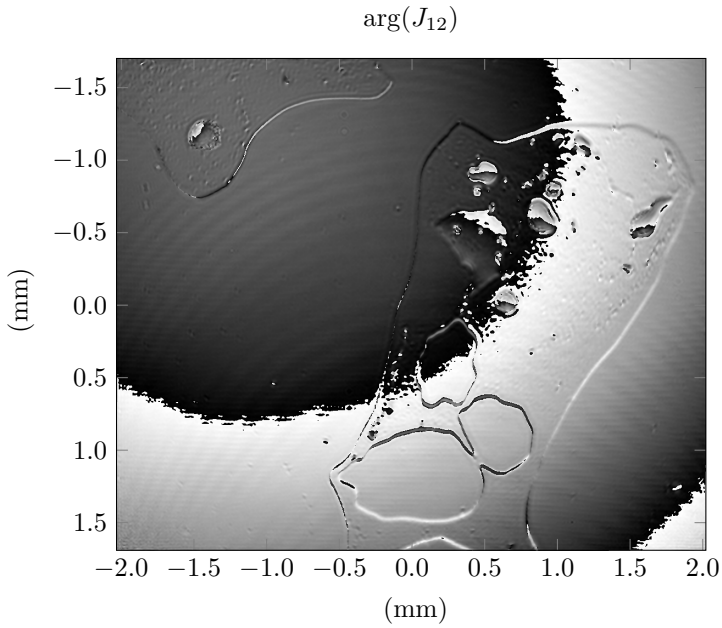

Figure 5.9: *Phase gradient. Extracted by filtering out all but the bottom lobe in figure 5.6 and taking the argument.*

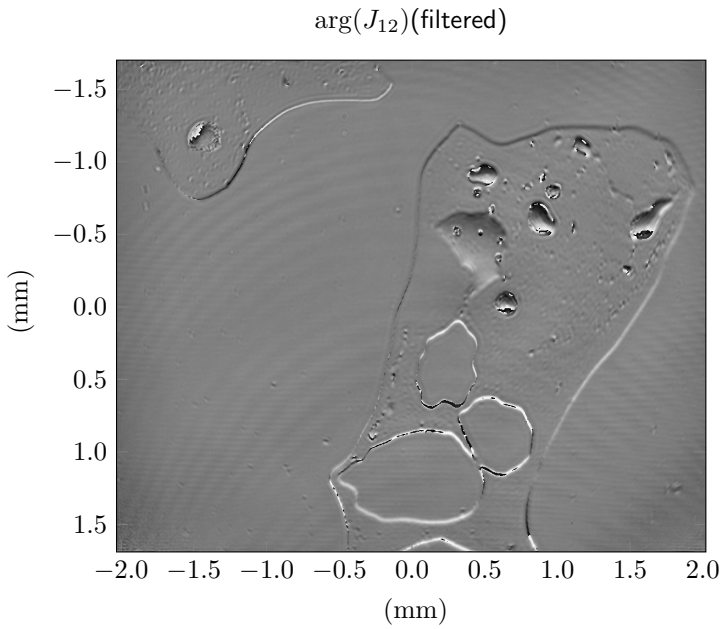

Figure 5.10: *Filtered phase gradient. Created by removing the low frequencies in J_{12} using an averaging filter.*

5.3 Correlation from shear

Here we check the behavior of the correlation from shear and its relation to the visibility. First the system was set in focus such that there was as little shear as possible. Because the experimental setup introduced a bit of rotation on the wavefronts, and the accuracy with which I could adjust the shear was limited, there remained some amount of significant shear in the image. The CCD was then moved back in steps of 1 mm from 0 mm to 13 mm. The camera stand was moved by hand and the defocus measured using a ruler, so some obvious imprecision in the defocus length has to be considered. Ten measurements was taken at each step for both a static and spinning diffuser. The object was that of water trapped between two glass plates. The parameters used can be found in table 5.2.

Parameters	
Wavelength λ	633 nm
Entrance pupil f_1	120 mm
Exit pupil f_2	250 mm
Beam width w	2 mm
Diffuser to object L	160 mm
Diffuser radius	35 mm
Diffuser speed	0 & 92.5 rpm
Exposure time	200 ms
Defocus Δz	0-13 mm
Limiting aperture	5 mm
Camera resolution	2048x2448 px
Pixel pitch	3.45x3.45 µm

Table 5.2: *Parameters used for the correlation measurements.*

We assume that the phase error for a single speckle pattern is much larger than the phase error for the sum of speckle patterns. This allows us to calculate the standard deviation of the phase from

$$\mathrm{std}\left(\arg(J_{12,single}J^*_{12,sum})\right), \tag{5.3-1}$$

where $J_{12,single}$ and $J_{12,sum}$ are the mutual intensities for the single speckle pattern and the sum of speckle patterns respectively. The result of this is plotted in figure 5.11a. One can see that the values for zero shear are erratic. This is probably due to something in the experimental setup getting moved slightly in between taking those measurements.

In figure 5.11b the standard deviation has been calculated to its corresponding correlation according to equation (4.2-4). A least square fit has been made for equation (4.1-17) where the data at zero shear has been excluded. As can be expected from section 4.4 these three figures and fits look very similar. Figure 5.11c and figure 5.11d show the visibility measured according to equation (4.4-7). No reference measurements have been made to remove disturbances. One can still see the relation between the correlation and visibility.

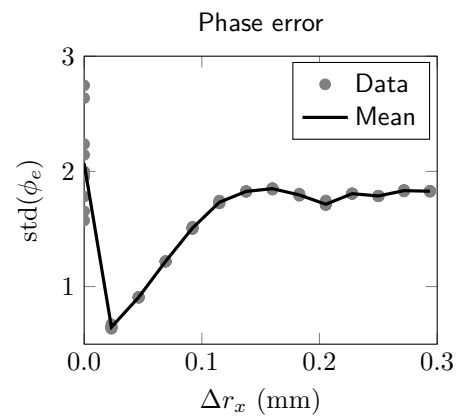

(a) *Standard deviation of phase error for a single speckle pattern.*

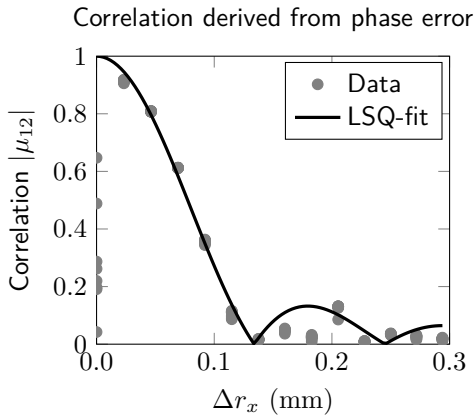

(b) *Correlation derived from the phase error using equation* (4.2-4)*.*

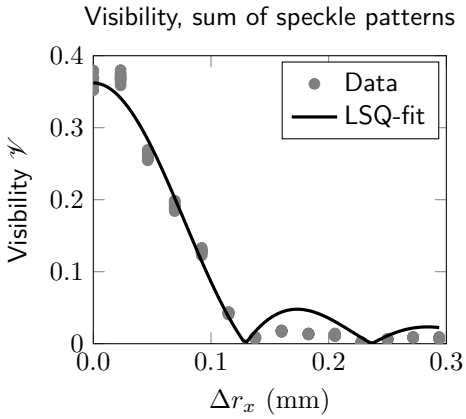

(c) *Visibility measured according to equation* (4.4-7) *for integration over multiple speckle patterns.*

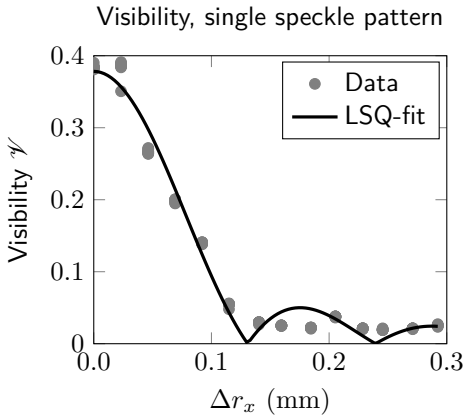

(d) *Visibility measured according to equation* (4.4-7) *for a single speckle pattern.*

Figure 5.11: *Variables related to correlation. The shear specified on the x-axes is relative to the object plane and corresponds to the defocus 0-13mm.*

5.4 Low correlation image

This is an example of how the image looks if we have very low correlation and visibility. The image corresponds to the data point in figure 5.11 closest to the first minimum. Figures 5.12 to 5.19 show two different measurements. The top figures show the image for when the diffuser is not spinning giving us a single speckle pattern. The bottom figures show the image for when the diffuser is spinning giving us a sum or integral of speckle patterns averaging out closer to the deterministic contributions to the complex wave function. List of parameters for these images can be found in table 5.3.

Parameters	
Wavelength λ	633 nm
Entrance pupil f_1	120 mm
Exit pupil f_2	250 mm
Beam width w	2 mm
Diffuser to object L	160 mm
Diffuser radius	35 mm
Diffuser speed	0 & 92.5 rpm
Exposure time	200 ms
Defocus Δz	7 mm
Limiting aperture	5 mm
Camera resolution	2048x2448 px
Pixel pitch	3.45x3.45 µm

Table 5.3: *Parameters used for the low correlation image*

In the spatial frequencies in figure 5.12 we can see a lot of higher frequencies. When looking at figure 5.13 we can see that they seem to have averaged out, probably due to them not being coherent. Looking at figure 5.15 we can see that as expected the center lobe is not affected by the low coherence. In figure 5.15 to figure 5.18 we can see that despite the low correlation it seems possible to see the deterministic contribution given enough uncorrelated speckle patterns.

For a very large shear like this the approximation that the phase difference equals the gradient is no longer a good one. That assumption assumes like any discrete gradient that the variation over the shear length is linear.

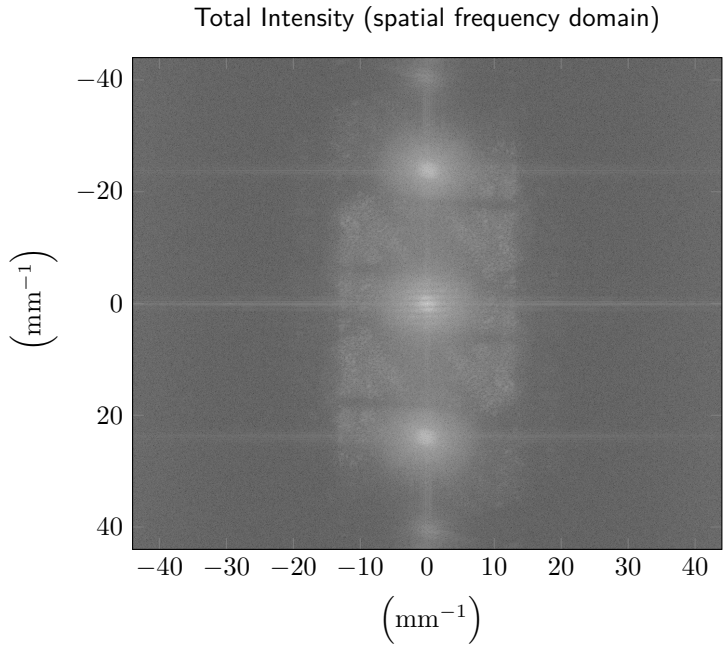

Figure 5.12: *Single speckle pattern. Spatial frequency domain of total intensity.*

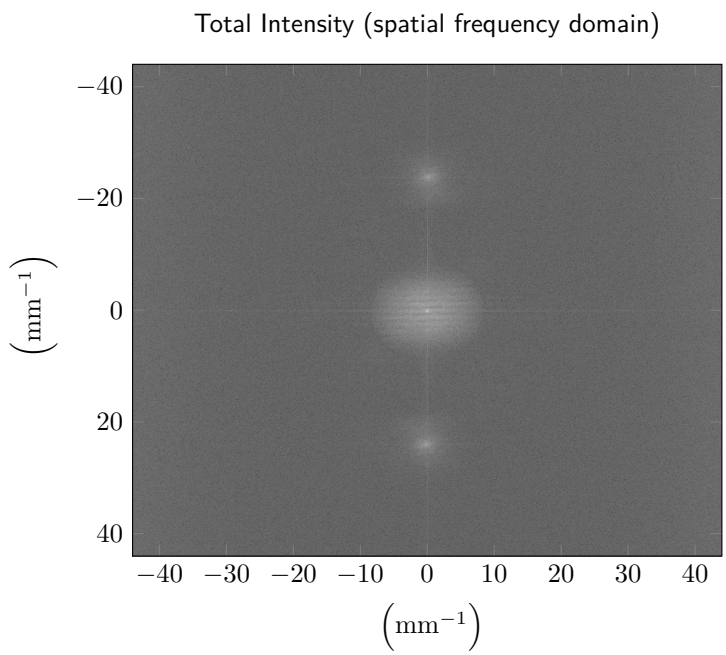

Figure 5.13: *Sum of speckle patterns. Spatial frequency domain of total intensity.*

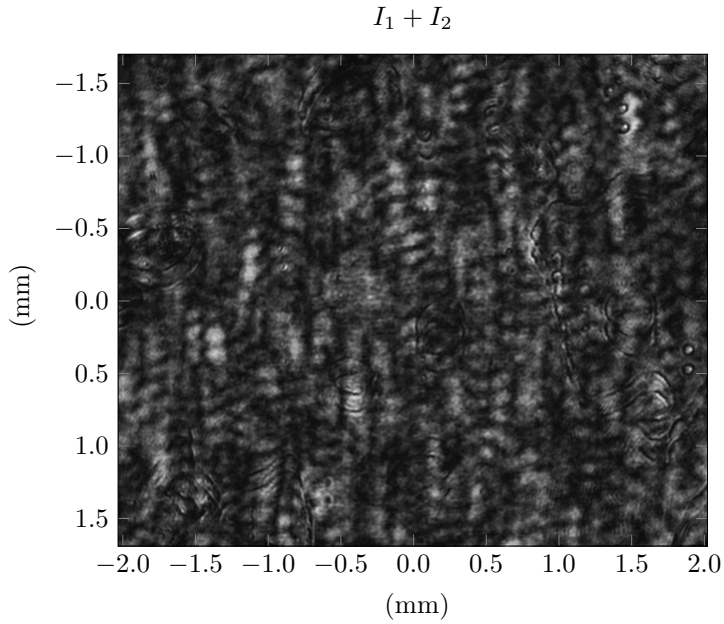

Figure 5.14: *Single speckle pattern. Sum of intensities. Extracted by filtering out all but the center lobe in figure 5.12.*

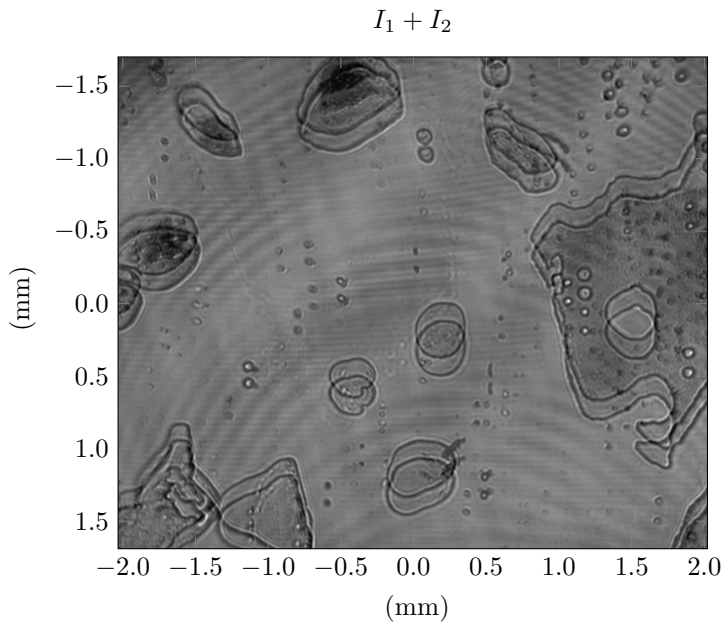

Figure 5.15: *Sum of speckle patterns.Sum of intensities. Extracted by filtering out all but the center lobe in figure 5.13.*

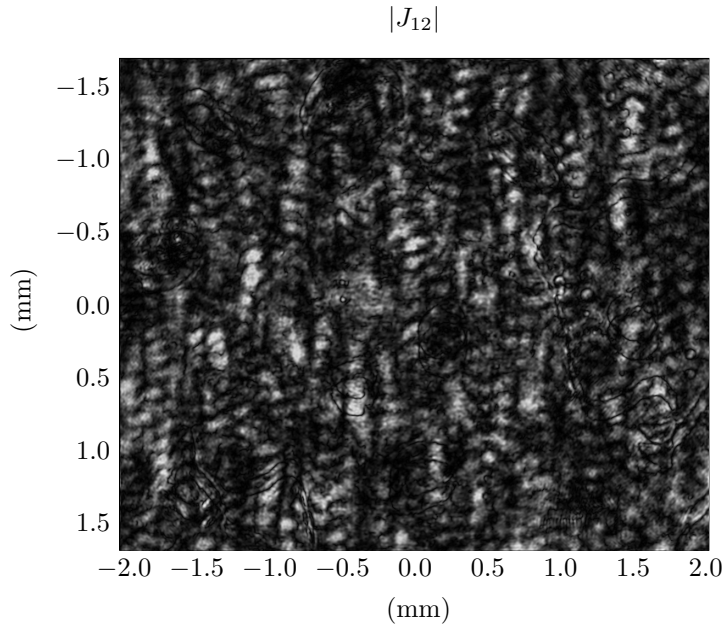

Figure 5.16: *Single speckle pattern. Absolute value of Mutual intensity. Extracted by filtering out all but the bottom lobe in figure 5.12 and taking the absolute value.*

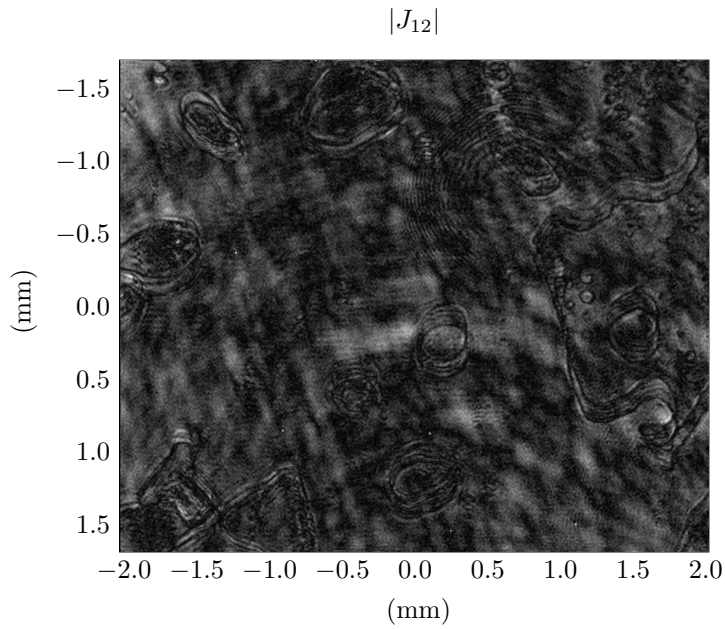

Figure 5.17: *Sum of speckle patterns. Absolute value of Mutual intensity. Extracted by filtering out all but the bottom lobe in figure 5.13 and taking the absolute value.*

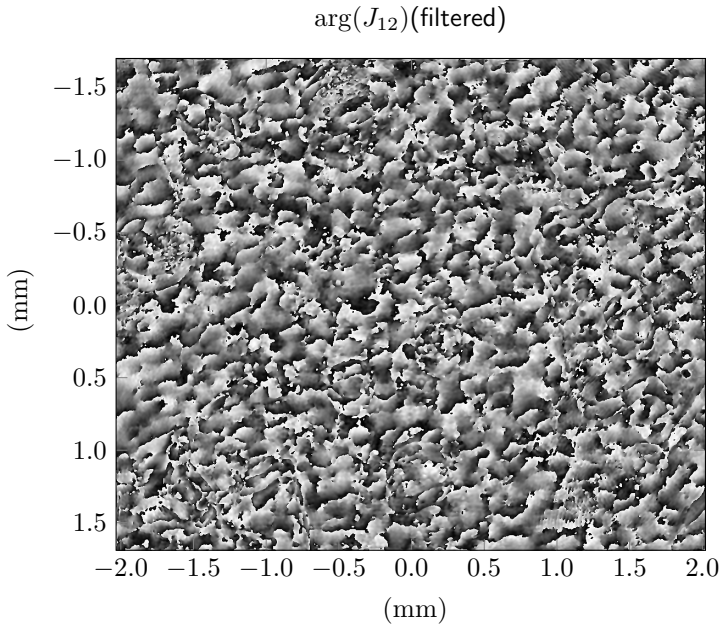

Figure 5.18: *Single speckle pattern. Phase gradient. Extracted by filtering out all but the bottom lobe in figure 5.12, taking the argument and removing low frequencies.*

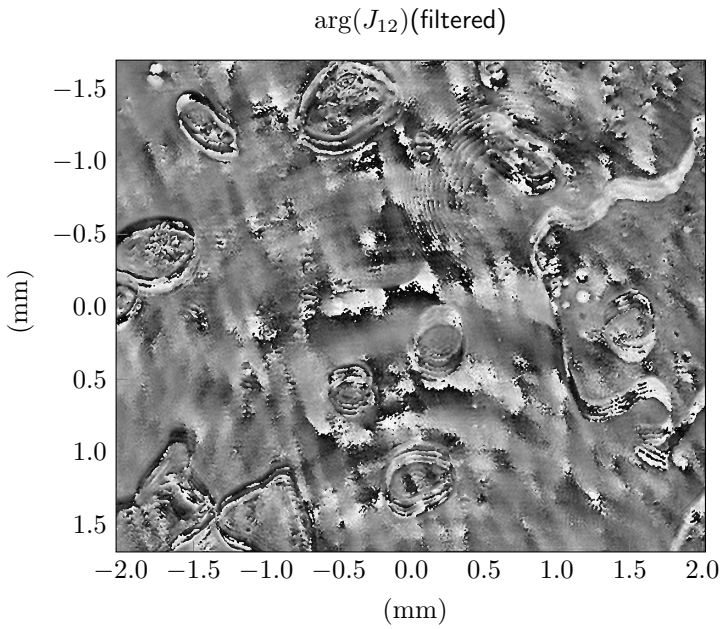

Figure 5.19: *Sum of speckle patterns. Phase gradient. Extracted by filtering out all but the bottom lobe in figure 5.13, taking the argument and removing low frequencies.*

CHAPTER 6

Discussion

6.1 Conclusions

The method shows some promise but with some limitations. One is that the aperture limits how low correlation you can have in the plane and still get a visible phase gradient. An early idea was that one might benefit from the numerical aperture being small, as it makes the light more coherent. But from the simulated results and some reasoning the system seems to benefit from having as large a numerical aperture as possible. The thesis does however not conclude that there can not be more complicated situations arising from a more complex aperture function or speckle bandwidth.

The most important parameters to consider for the image quality is how the spatial bandwidth relate to the aperture, and how the correlation relate to the number of uncorrelated speckle patterns. Other parameters such as visibility can have an effect but it is the previous two relations that should be one's primary concern when designing an implementation for this system.

The experiments do show very smooth phase gradients. They also show that one does not require too much in way of correlation and visibility to get a decent phase gradient. Finally the experiments show that the simulation and analytical expressions seem to be reasonable.

The simulation can thus be considered successful. More options could always be added, but with more options comes more input. Optimizations documented reflects the most useful ones for implementations of similar systems in Matlab.

6.2 Further research

In this thesis there has only been a look at square and circular speckle bandwidths and apertures. As we are looking at the gradient of the phase low frequencies are not very interesting. So using an aperture that lets a larger part of lower frequencies through might not be an optimal design. To complement a more wild aperture it could also

be an idea to shape your speckle bandwidth to optimize the amplitude of interesting frequencies passing through.

The simulation can be expanded to work for 3-dimensional inputs. The simulation does already support vectorization of multiple plane waves, but is missing support for defocus in the object plane and assigning different defocus lengths for different depths of a 3D-structure. With a simulation working for 3-dimensional inputs one could also look at the effect of longitudinal shear on the system. It could also give a better simulation of the lateral shear when using defocus as you get the effect of different focus planes.

As the simulation supports it one could also study systems which splits the wavefront into more than three parts. One of the linked references is to an article about a method with four-way lateral shear.

References

[1] F. Zernike, "Phase contrast, a new method for the microscopic observation of transparent objects," *Physica*, vol. 9, pp. 686–698, July 1942.

[2] S. Bernet, A. Jesacher, S. Fürhapter, C. Maurer, and M. Ritsch-Marte, "Quantitative imaging of complex samples by spiral phase contrast microscopy," *Optics Express*, vol. 14, no. 9, pp. 3792 – 3805, 2006.

[3] E. Cuche, F. Bevilacqua, and C. Depeursinge, "Digital holography for quantitative phase-contrast imaging," *Opt. Lett.*, vol. 24, pp. 291–293, Mar 1999.

[4] Y. Sung, W. Choi, C. Fang-Yen, K. Badizadegan, R. R. Dasari, and M. S. Feld, "Optical diffraction tomography for high resolution live cell imaging," *Optics Express*, vol. 17, no. 1, pp. 266 – 277, 2009.

[5] B. W. P. Bon, G. Maucort and S. Monneret, *Quadriwave lateral shearing interferometry for quantitative phase microscopy of living cells*. Optics express 17(15), 2009.

[6] R. Mäki, *Three-wave Lateral Shearing Interferometry For Quantitative Phase Imaging*. Project in F7024T, LTU, 2014.

[7] K. D. Möller, *Optics. [electronic resource] : Learning by Computing, with Examples Using Mathcad®, Matlab®, Mathematica®, and Maple®*. New York, NY : Springer Science+Business Media, LLC, 2007., 2007.

[8] A. Barty, K. A. Nugent, D. Paganin, and A. Roberts, "Quantitative optical phase microscopy," *Opt. Lett.*, vol. 23, pp. 817–819, Jun 1998.

[9] J. W. Goodman, *Statistical Optics*. John Wiley & Sons, Inc, 1985.

[10] B. E. Saleh and M. C. Teich, *Fundamentals of Photonics*. John Wiley & Sons, Inc, second ed., 2007.

[11] R. N. Bracewell, *The Fourier Transform and Its Applications*. McGraw-Hill Book Company, revised second ed., 1986.

[12] P. K. Rastogi, *Digital Speckle Pattern Interferometry and Related Techniques*. John Wiley & Sons, Ltd, 2001.

[13] J. W. Goodman, *Introduction to Fourier Optics*. McGraw-Hill Book Company, 1985.

APPENDIX A

Matlab Code

Listing A.1: Normalized cross correlation function

```
function g = xcorr2_normalized( A, B, maxlag )
%XCORR2_NORMALIZED Normalized version of xcorr2
%
%   XCORR2_NORMALIZED(A,B) computes the crosscorrelation of
%   matrices A and B.
%   XCORR2_NORMALIZED(A) is the autocorrelation function.
%
%   maxlag will only work as intended for matrices dim(A) = dim(B),
%   it is called as below:
%
%   XCORR2_NORMALIZED(A,B,maxlag) computes the crosscorrelation of
%   matrices A and B with maxlag.
%   XCORR2_NORMALIZED(A,[],maxlag) is the autocorrelation function
%   with maxlag.

    function I = intensity_matrix(X, n_X, m_X, n_Y, m_Y)
        %Calculates the intensity for X at each point in the
        %cross-correlation matrix.
        I(n,m) = 0;
        I(1:n_X, 1:m_X) = cumsum(cumsum(abs(X).^2,1),2);
        I(n_X+1:end, :) = repmat(I(n_X,:),n-n_X,1);
        I(:, m_X+1:end) = repmat(I(:,m_X),1,m-m_X);
        I(n_Y+1:end,:) = I(n_Y+1:end,:) - I(1:n_X-1,:);
        I(:,m_Y+1:end) = I(:,m_Y+1:end) - I(:,1:m_X-1);
    end

if ~exist('B','var') || isempty(B)
    [n_A, m_A] = size(A);
    n = 2*n_A - 1;
    m = 2*m_A - 1;
    B = A;
```

```
32      I_A = intensity_matrix(A, n_A, m_A, n_A, m_A);
33      I_B = I_A;
34  else
35      [n_A, m_A] = size(A);
36      [n_B, m_B] = size(B);
37      n = n_A + n_B - 1;
38      m = m_A + m_B - 1;
39      I_A = intensity_matrix(A, n_A, m_A, n_B, m_B);
40      I_B = intensity_matrix(B, n_B, m_B, n_A, m_A);
41  end
42
43  if ~exist('maxlag','var')
44      shape = 'full';
45  else
46      %Reshape intensity matrices for the set maxlag.
47      subn = (n-1)/2+(-maxlag:maxlag) + 1;
48      subm = (m-1)/2+(-maxlag:maxlag) + 1;
49      I_A = I_A(subn, subm);
50      I_B = I_B(subn, subm);
51      %Use conv2 'valid' option to limit the lag.
52      shape = 'valid';
53      A = padarray(A, [maxlag maxlag]);
54  end
55
56  %Calculate cross-correlation
57  g = conv2(A, rot90(conj(B),2), shape);
58  %Normalize
59  g = g./(I_A.*rot90(conj(I_B), 2)).^(0.5);
60
61  end
```

Listing A.2: Shear imaging

```
1   function [U,X,Y]=shear_imaging(d,lambda,z1,z2,f,NA,A,...
2       dx,dy,dsx,dsy,IRel,Ap)
3
4   % [U,X,Y] = SHEAR_IMAGING(d,lambda,z1,z2,f,NA,A,...
5   %   dx,dy,dsigx,dsigy,IRel,Ap)
6   % Calculates the complex amplitude of a laterally sheared
7   % image close to the image plane.
8   %
9   % INPUT:
10  %
11  % d is the source pixel size,
12  % lambda the wavelength,
13  % z1 the propagation distance before the principle planes,
14  % z2 the propagation distances after the principal planes,
15  % f is the focal length.
16  %
17  % NA is the numerical aperture,
18  % A is the complex amplitude in the source,
19  %
20  % dx is a vector with the shear in x,
21  % dy is a vector with the shear in y,
22  % dsx is a vector with the frequency shift in x,
23  % dsy is a vector with the frequency shift in y,
24  % IRel is a vector with the relative intensity between the components
25  %
```

```
26  %
27  % d, lambda, z1, z2, f, dx and dy should be in the same unit.
28  % NA, dsx, dsy is in units of directional cosines.
29  %
30  % dx, dy, dsx, dsy and IRel
31  % should contain all the same number of elements.
32  %
33  % Ap is optional, set Ap to 'square' to use a square aperture.
34  % By default the aperture is circular.
35  %
36  % OUTPUT:
37  %
38  % U is the complex amplitude close to the image plane,
39  % it will have dimensions size(U) = N x M x size(A,3),
40  % such that no aliasing occur for the
41  % intensity of U: I = U.^2;
42  % X and Y maps the spatial coordinates to the vectors of size N and M
43  % respectively.
44  %
45  % EXAMPLE, Three-way lateral shear:
46  %
47  % d = 1e-6;
48  % lambda = 500e-9;
49  % z1 = 1;
50  % z2 = 2;
51  % f = 1/(1/z1 + 1/z2);
52  % NA = 0.02;
53  % A = fft2(randn(512,512,10) + 1i*randn(512,512,10));
54  % dx = [0, 3, 0];
55  % dy = [0, 0, 3];
56  % dsx = 2*NA*[-1, -1, 1];
57  % dsy = 2*NA*[-2, 2, -2];
58  % IRel = [2, 1, 1];
59  % Ap = 'circ';
60  %
61  % [U,X,Y] = shear_imaging(d,lambda,z1,z2,f,NA,A,...
62  %   dx,dy,dsx,dsy,IRel,Ap);
63  % I = sum(abs(U).^2, 3); %Sum up intensities
64  % imagesc(X,Y,I)
65
66  %% Physical variables
67  k=2*pi/lambda;       % angular wavenumber
68  L=f*z1/(z1-f);       % position of the image plane
69  M=L/z1;              % Magnification between object and image plane
70  dz=z2-L;             % Defocus distance
71  AmpRel = sqrt(IRel/sum(IRel)); % Normalized relative amplitudes
72
73  %% Calculation grids
74  n_A=size(A,1); % Original grid size
75
76  %Aperture
77  n_Um = ceil(2*NA*n_A*d/lambda); %Aperture grid size
78  d_Um = d*n_A/n_Um; %pixel pitch aperture
79  c_Um = floor(n_Um/2); %center px aperture
80
81  %Frequency shift in px
82  dax = fix(dsx*(n_Um*d_Um)/lambda);
83  day = fix(dsy*(n_Um*d_Um)/lambda);
84
```

```
%Output
n_U = 2*n_Um+2*max([max(dax)-min(dax) max(day)-min(day)]);
%Output grid size
d_U = M*d*n_A/n_U; %pixel pitch output image
c_U = floor(n_U/2); %center px image

%% Aperture function
A = fft2(A);

%Limit A to only fit aperture frequencies
Um = A([1:c_Um, (end-c_Um+1):end],[1:c_Um, (end-c_Um+1):end],:);

ax_Um = [0:(c_Um-1) -c_Um:-1]; %matlab fft mapping
sx_Um = lambda*ax_Um/(n_Um*d_Um);

%Circular aperture (default)
if ~(exist('Ap','var') && isequal(Ap, 'square'))
    st2 = bsxfun(@plus, sx_Um.^2, (sx_Um').^2);
    Um = bsxfun(@times, Um, st2<NA^2);
end

%Multiply with all constants when the matrix is at its smallest
%Phase, magnification and fft2 scale factor
Um = Um*(exp(1i*k*L)/(M*numel(A)));

%% Create wave with sheared components
U = zeros(n_U, n_U, size(A,3));

%Maps the frequencies in Um with frequency shift dsig to U
    function M = map(da)
        M = [1:c_Um (n_U-c_Um+1):n_U]';
        M = M + da; %shift
        M(M<=0) = n_U + M(M<=0); %wrap negative indices
        M(M>n_U) = mod(M(M>n_U),n_U); %wrap indices >n_U
        M(M==0) = n_U;
    end

% Add components
for ii = 1:numel(IRel)
U(map(day(ii)), map(dax(ii)),:) =...
    U(map(day(ii)), map(dax(ii)),:) +...
    AmpRel(ii)*bsxfun(@times, Um,...
    (exp(-1i*k*dy(ii)*sx_Um')*exp(-1i*k*dx(ii)*sx_Um)));
end

%% Diffract
% diffract here instead of performing unecessary extra FFTs
ax_U = [0:(c_U-1) -c_U:-1];
sx_U = lambda*ax_U/(2*c_U*d_U);
sz = (bsxfun(@minus, 1-sx_U.^2, (sx_U.^2)')).^(0.5);
U = bsxfun(@times, U, exp(1i*k*dz*sz));

%% Output
U=fft2(U);
X=d_U*(-c_U:(c_U-1)); %Spatial mapping
Y=X;

end
```